Sensors & Diagnostics

CRITICAL REVIEW

View Article Online
View Journal | View Issue

Cite this: *Sens. Diagn.*, 2023, **2**, 507

Surface acoustic wave based microfluidic devices for biological applications

Xianglian Liu, Xuan Chen, Ziwei Yang, He Xia, Chuanyu Zhang and Xueyong Wei *

Over the past decade, surface acoustic wave (SAW) devices have been widely used in the field of biological detection, including as actuators for sample pretreatment processes and as biosensors for the qualitative or quantitative detection of various biological objectives, with favorable biocompatibility, contactless operation, and noninvasive features. In this review work, we choose types of SAWs as the thread to run through various implements. The theoretical basis is firstly explained to provide the physical principles governing the design and operation of SAW in the above fields. Also, the notable set-ups and key features in each category are summarized and discussed in detail, allowing rapid access to specific advancements for researchers in the field. Finally, the perspectives on the future trend in terms of opportunities and challenges of SAW-based detection devices are offered.

Received 13th November 2022,
Accepted 16th March 2023

DOI: 10.1039/d2sd00203e

rsc.li/sensors

1. Introduction

Microfluidic chips have attracted much attention in the area of biosensors. Due to their ability to deal with very small amount of samples and reagents accurately, such as separation and mixing, microfluidic chips are excellent platforms to carry out detections with high resolution and sensitivity.[1] The small size, low cost, and automation of microfluidic chips offer new capabilities for analytical devices.[2,3] To precisely manipulate the fluids inside microchannels, techniques such as electrowetting,[4] magnetics,[5] and optics[6] are widely incorporated in microfluidics. In recent years, there has been a considerable progress in the application of surface acoustic waves (SAWs) on miniatured devices for life science, which will be presented in detail and summarized in this review.

SAWs are elastic waves travelling along the surface of piezoelectric materials, which were firstly discovered in 1885 by Lord Rayleigh.[7] Until 1965, the phenomenon of SAWs propagation was figured out by White and Voltmer and the first interdigital transducers (IDTs) were made.[8] An interdigital transducer (IDT) consists of two interlocking comb-shaped metal electrodes, deposited on a piezoelectric material. When a sinusoidal wave is applied, the piezoelectric material beneath IDTs will vibrate due to the inverse piezoelectric effect, and an acoustic wave perpendicular to the IDTs will be generated and electric energy is transferred to acoustic energy. Unlike SAWs, bulk acoustic waves (BAWs) travel throughout the medium. When the piezoelectric

State Key Laboratory for Manufacturing Systems Engineering, Xi'an Jiaotong University, Xi'an, 710049, PR China. E-mail: seanwei@mail.xjtu.edu.cn

Xianglian Liu

Xianglian Liu is currently a Ph.D student at the State Key Laboratory for Mechanical Manufacturing Systems Engineering, Xi'an Jiaotong University, China. Her research interest is in acoustic microfluidics and biosensors.

Xuan Chen

Xuan Chen is currently a Ph.D student in at State Key Laboratory for Mechanical Manufacturing Systems Engineering, Xi'an Jiaotong University, China. Her research interest is in nanomaterials and biosensors.

material is activated, the acoustic waves will enter the microchannel through the solid–liquid interface. The acoustic waves will resonate inside the channel as long as the characterize size, such as width, is an integral multiple of the semi-wavelength, hence forming a resonance chamber. The reflection of acoustic waves from the wall of the microchannel leads to the appearance of BAWs.[9] Two key factors influencing the BAW propagation are the acoustic impedance of the substrate and the quality factor of the resonance chamber.[10] The devices of BAWs usually utilize quartz crystal microbalances (QCM), consisting of a bulk of quartz crystal sandwiched between two gold electrodes.[11] Since the acoustic wave penetrates only a wavelength in depth, the energy density is quite high on the surface. SAW has extremely low wave velocity in piezoelectric material and very short wavelength, which is 10^5 times smaller than that of the electromagnetic wave.[12] Therefore, for the same frequency band, the size of SAW devices is much smaller than the electroacoustic wave devices.[12,13]

Within half a century, surface acoustic wave (SAW) devices have been widely used in wireless communication,[14,15] radio and television,[16,17] mesoscopic systems,[18,19] quantum acoustics,[20,21] and a variety of sensors,[22–31] including gas,[22,27] chemical vapor,[31] temperature,[23] humidity,[29] biology,[24–26] pressure,[28] and contaminants.[30] In terms of electrode structures for SAWs-based sensors, they usually consisted of a pair of IDTs with opposite directions, where one served as the input IDT and the other served as the output part. Since the velocity of the SAWs is highly dependent on the changes in surface temperature, viscosity, and mass loading, SAWs-based sensor is an excellent choice for biological sensing in aqueous environments. The change in SAWs velocity between the input and output IDTs will be characterized by the phase shift and amplitude difference, which are presented by an oscillating electric signal from output based on the piezoelectric effect.[32] It is also worth mentioning that SAWs have been used extensively in electronic communications such as cell phones for signal processing and filtering,[33] demonstrating that the devices of SAWs are highly compact, reliable, and low-priced, including the driving circuits and power supplies. Moreover, the power intensity of SAWs is proved to be safe for biological molecules and organisms,[34]

Ziwei Yang

Ziwei Yang is currently a Ph.D student at the State Key Laboratory for Mechanical Manufacturing Systems Engineering, Xi'an Jiaotong University, China. Her research interest is in nanomaterials and biosensors.

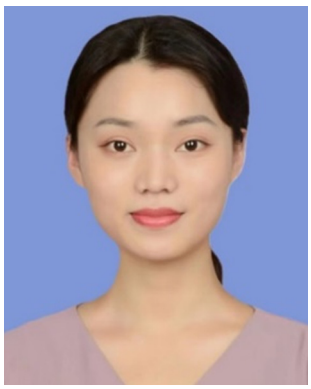

He Xia

He Xia is currently a Ph.D student at the State Key Laboratory for Mechanical Manufacturing Systems Engineering, Xi'an Jiaotong University, China. Her research interest is in nanomaterials and biosensors.

Chuanyu Zhang

Chuanyu Zhang is currently a post-doctoral candidate at the State Key Laboratory for Mechanical Manufacturing Systems Engineering, Xi'an Jiaotong University, China. His research interest is in acoustofluidics and microfluidics.

Xueyong Wei

Xueyong Wei received his M.S. degree in Xi'an Jiaotong University in 2005 and his Ph.D. degree in University of Birmingham in 2009. He then conducted research on micromechanical inertial sensors at the University of Cambridge as a post-doctoral research associate. He joined the faculty of Mechanical Engineering Department at the Xi'an Jiaotong University in 2012, where he is presently a professor in Microsystems Technology. His research interests include micromechanical resonators and oscillators, MEMS sensors, and microfluidics.

ensuring that this technique has high biocompatibility. Another non-negligible advantage of SAW is that this technology is completely contact-free. For example, when combined with microfluidics, SAW can not only control the liquid (such as mixing, jetting, translation, and atomization) but also manipulate particles from nanometer to millimeter scale without any risk of sample contamination.[35] Considering the above advantages, SAW devices have been widely used in the field of biological detection, including as actuators for sample pretreatment process and as biosensors for the qualitative or quantitative detection of various biological objectives.

In this work, the SAW microfluidic devices for biological application are summarized according to the type of SAW, including Lamb waves, love mode wave SAW (LW-SAW), Rayleigh SAW, and shear-horizontal SAW (SH-SAW) categorized by the difference in the acoustic vibration modes and boundary conditions. As listed in Fig. 1, Rayleigh SAW-based devices are ordinarily applied as actuators in separation, sorting, concentration of biological particles, and liquid mixing. In contrast, devices based on other SAWs are mostly used as biosensors for the detection of various biological objectives, such as biomolecules, cells, viruses, and bacteria.

2. Basics of SAWs

SAWs can be divided into different types depending on their acoustic vibration modes, propagation medium, and boundary conditions. On semi-infinite substrates, Rayleigh SAW, leaky SAW, shear-horizontal SAW (SH-SAW), and Lamb SAW can be generated; on the other hand, on substrates with layered structure, love mode wave SAW (LW-SAW), Sezawa SAW, and Stoneley SAW can be generated,[36,37] in which Rayleigh SAW, SH-SAW, LW-SAW, and Lamb wave are more commonly used in biology sensing and will be discussed in detail in the following sections. We try to offer just enough coverage of relevant mathematics so that one access many models built for various SAWs phenomena. However, a complete coverage of this topic might overwhelm the scope of this work. Herein, some classical and key mathematical descriptions are summarized.

The typical SAW device is composed of a piezoelectric material substrate with IDTs deposited and a microchannel bonding on the substrate. The wavelength of SAWs is dependent on the structure of IDTs, which can be calculated as:[38]

$$\lambda = 4d \tag{1}$$

where λ is the wavelength of SAWs and d is the width of IDTs (assuming the width and the spatial distance of IDTs are the same). The acoustic frequency f can be calculated as:[38]

$$f = v/\lambda \tag{2}$$

where v is the speed of sound in the piezoelectric substrate.

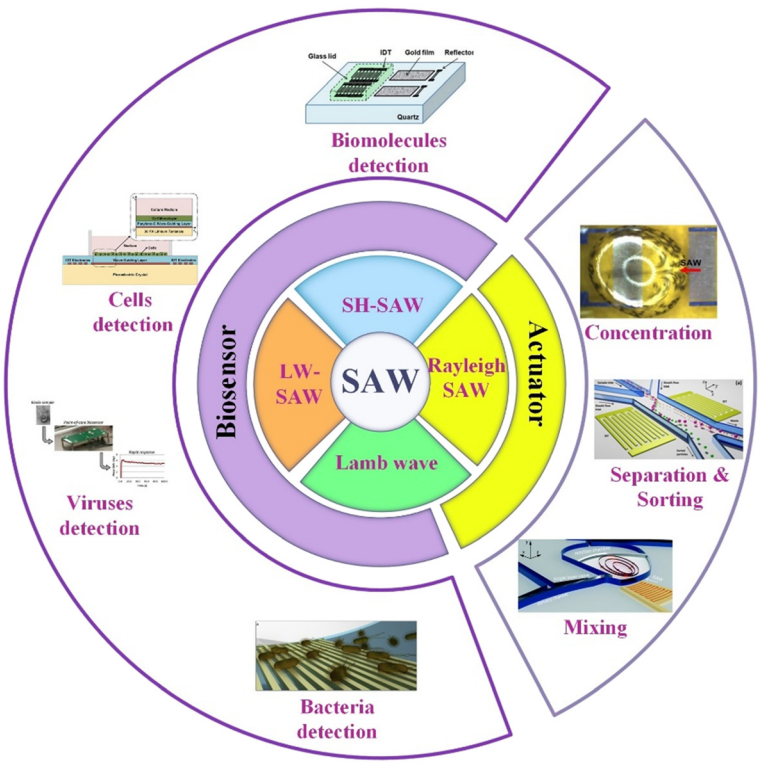

Fig. 1 The SAW devices for biological applications.

The amplitude of SAWs attenuates exponentially when transmitting through the channel wall. Since the propagation speeds of SAW varied in fluids and substrate, a part of SAWs refracts into the liquid in the form of longitudinal waves with a refraction angle, which is known as the Rayleigh angle.[38]

$$\theta = \arcsin(c_1/c_s) \tag{3}$$

where c_1 and c_s are the acoustic wave velocities in the substrate and the fluid, respectively. The SAWs transmitted into the microchannel are also called "leaky SAWs" because of this acoustic refraction.[35] Notably, due to the anisotropy of piezoelectric materials, the acoustic wave velocities of the same material in different tangential directions are different. Correspondingly, the Rayleigh angle varies with the different tangential direction of the substrate.[36]

The propagation of acoustic waves is a flow of wave energy. When the wave flow is interrupted, the acoustic radiation pressure will apply a force to the object in the direction of propagation.[39] The force is a nonlinear effect, which cannot be analyzed by linear acoustics. This effect is caused by the viscous attenuation feature of the fluid.[40] Radiation force provides the foundation for SAWs to manipulate the particles and fluidics at the microscale.

For particles far from the channel wall moving with a certain velocity v_p, the viscous drag force can be calculated by Stokes' law[41]

$$F_d = 6\pi a\mu(v_f - v_p) \tag{4}$$

where v_f and μ are the velocity and viscosity of fluid respectively, and a is the diameter of particles. Conditions for Stokes' law to work are: the fluid follows laminar flow, particles are smooth, spherical, and have uniform size, and there is no interaction between particles.

Meanwhile, the scattering of the incident acoustic wave will exert a radiation force on the particles, and the acoustic radiation force will drive the particles in the fluid to move. The acoustic radiation force F_r acting on particles in the inviscid fluid is defined as:[42]

$$F_r = -2\pi {r_p}^3 \rho_l \nabla\left(\frac{1}{3} f_1 \frac{{p_l}^2}{{p_l}^2 {c_l}^2} - \frac{1}{2} f_2 {v_l}^2\right) \tag{5}$$

$$f_1 = 1 - \frac{\beta_p}{\beta_l};\ \ f_2 = \frac{2\left(\rho_p - \rho_l\right)}{2\rho_p + \rho_l} \tag{6}$$

where ${p_l}^2$ and ${v_l}^2$ are the average value of the square of pressure and velocity in a single acoustic period, c_l, β_l, ρ_l, and c_p, β_p, and ρ_p are acoustic wave velocity, compressibility, and density of the liquid and particles, respectively.[43]

It must be recognized that this equation can only describe the acoustic radiation force of single particle in the fluid, ignoring the refraction and reflection from other components in the fluid environment. The acoustic interaction between these particles will produce secondary acoustic forces if there are other particles in the fluid.[44] It should be noted that particles in the fluid are under the action of viscous drag force and acoustic radiation force simultaneously, and which of these is the dominant force is determined by the size of particles. This size threshold depends on factors including acoustic wave frequency, acoustic wave contrast factor, and kinematic viscosity.

3. Bioparticle manipulation based on Rayleigh SAW

Rayleigh wave propagates along a solid surface, including longitudinal (P) and shear vertical (SV) wave components. The surface particles move in an elliptical fashion, normal to the surface and parallel to the direction of propagation. Meanwhile, the motion amplitude decreases exponentially with the substrate depth.[45] For Rayleigh wave generation, as its disturbance is confined to surface layers, the power consumption is lower. Also, it can be also of low cost as it is relatively easy to fabricate, such as through metal deposition on the surface of piezoelectric material (IDTs), which can satisfy the excitement requirement in many situations. Rayleigh wave is used widely in the sorting of biological particles, such as cells, proteins, microorganisms, and exosomes. Except for separation, the Rayleigh wave is also widely applied in enrichment,[46] mixing,[47] heating,[48] *etc.* A standing surface acoustic wave (SSAW)-based microfluidic device was developed for non-contact, continuous cell enrichment and was able to concentrate highly diluted blood cells by more than 100 folds with a recovery efficiency of up to 99%.[46] The synergic combination of SAW-mixing and SAW-sensing was shown and characterized, with an application to detect measles virions (MV) in clean buffers and loaded in healthy whole human saliva.[47] It was suggested that the SAW-induced acoustic mixing and the mixing in microfluidic devices in general should be implemented to achieve the best biosensing performance in terms of sensitivity and selectivity. Roux-Marchand *et al.*[48] studied the temperature uniformity of a microdroplet heated by Rayleigh surface acoustic wave for discrete microfluidic applications such as biological reactions. It was shown that the applied power, SAW wavelength, and microdroplet volume influence the heating uniformity of the microdroplet.

Traditional sample processing methods, including centrifugation, electrophoresis, and filtration, require complex process and bulky equipment. SAW separation techniques have various advantages including low energy consumption, low cost, simple, biocompatibility, as well as contactless and non-invasive features.[49] Thus, acoustofluidic separation has become a very promising alternative used in research and clinical applications including micron-sized cells and submicron bioparticles.

There are two kinds of Rayleigh SAW devices according to the separation principle, as shown in Fig. 2.[50] Traveling surface acoustic waves (TSAWs) are generated by IDTs on one side, which are flexible to manipulate and generate acoustic

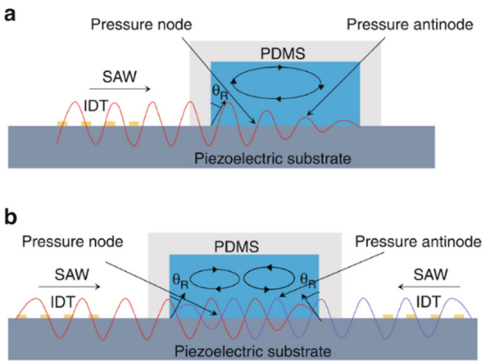

Fig. 2 Schematic diagrams of different types of surface acoustic waves. a: Acoustic streaming effect of traveling surface acoustic waves (TSAWs); b: acoustic streaming effect of standing surface acoustic waves (SSAWs).[50]

streaming to separate particles. Standing surface acoustic waves (SSAWs) are generated by two opposite IDTs, creating the convenient control of particles by pressure nodes and antinodes.

3.1 TSAW-based separation

TSAW is generated by IDTs on one side, allowing SAWs propagate in one direction and moving the fluid and particles away from the IDTs. Particles with different sizes experience different acoustic radiation force and drag force. Whether acoustic streaming flow-induced drag force or acoustic radiation force is the main force driving the motion of the particles depends on the size of particles. When the perimeter of the particle is smaller than the fluid wavelength, acoustic streaming flow-induced drag force plays a leading role. On the other hand, the acoustic radiation force pushes the particles mainly when the perimeter of the particle is larger than the fluid wavelength.

3.1.1 Separation of cells. Label-free cell separation methods are based on the inherent properties such as size. Lu *et al.*[51] showed a label-free platform for the isolation of cancer cells (>10 μm) from biological samples making use of arrays of acoustic microstreaming traps surrounding the micropillar in FTSAW. The versatile and reversible properties of the acoustic microstreaming ensure the capture and release of cancer cells. Isolation efficiency of 95% was obtained in the spiked saline buffer and diluted serum and of 66 ± 4% in whole blood samples (Fig. 3a).

Cells of similar size lack sufficient sorting specificity to allow their distinction from other normal cells in blood. Therefore, surface biomarker-based cell sorting and fluorescence activated cell sorting (FACS) techniques are widely exploited in cell separation.

Liu *et al.*[52] used size-amplifiers (40 μm-diameter anti-EpCAM/gelatin-coated SiO_2 microbeads) bound to circulating tumor cells (CTCs) to amplify the physical differences (size and mechanics) between CTCs and normal blood cells. The amplified acoustic radiation force generated by TSAW (19.9 MHz) can be approximately hundredfold over that of bare CTCs or normal blood cells, resulting in the efficient sorting of CTCs bound to size-amplifiers out of the blood samples, with a total efficiency of ~77%, purity of 96%, and viability of 83%. Ma *et al.*[53] used a highly focused traveling surface acoustic wave (FTSAW) beam with a width of ~50 μm and resonance frequency of 132 MHz to sort out MCF-7 breast cancer cells from diluted whole blood samples with a purity of 86% and viability of 95%. The fluorescence detection will trigger the IDTs to sort the target cells from heterogeneous populations (Fig. 3b). This group further developed a method combining inertial focusing and fluorescence-activated acoustic sorting for single cell isolation at ~kHz rates. Inertial focusing completed the pre-enrichment and after FTSAW sorting, at least 2500-fold purity enrichment of the MCF-7 breast cancer cells spiked in diluted whole blood samples with cell viability maintained at 91% (viability before sorting was 94%) can be obtained.[54] Mutafopulos *et al.*[55] employed FACS with tapered IDTs and inertial flow focusing to sort three different cell lines at several kHz with purity

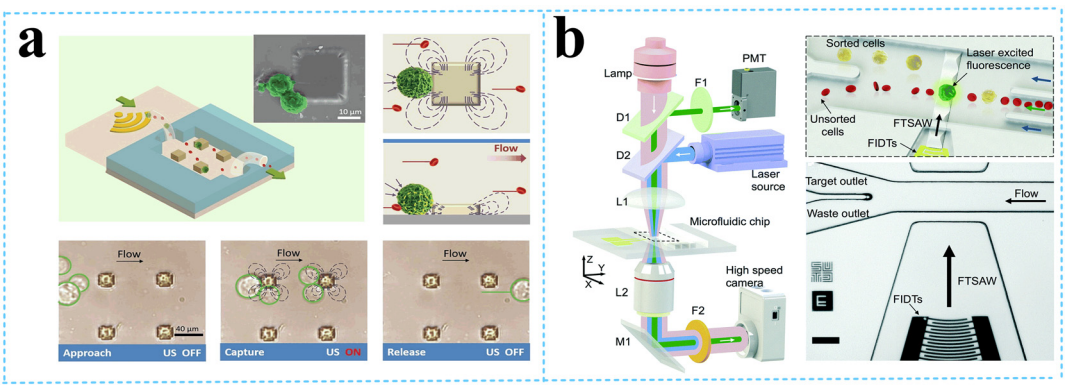

Fig. 3 Separation of micron-sized cells in TSAW devices for cell separation. a: Schematic of a parallel isolation microdevice for isolating cancer cells (green) from a biological fluid containing numerous red blood cells (red) (reproduced from ref. 51 with permission from WILEY-VCH Verlag GmbH & Co. KGaA, copyright 2018); b: schematic of the optical set-up and fluorescence activated sorting process of MCF-7 breast cancer cells in the FTSAW sorting chip (reproduced from ref. 53 with permission from the Royal Society of Chemistry, copyright 2017).

and cell viability of about 90% simultaneously. The inertial flow focusing aligns and evenly spaces cells, thus improving the efficiency, and the tapered IDTs can be tuned by the radio frequency generator signal of 162 to 164 MHz to adjust the TSAW position. Ung *et al.*[56] designed a multi-layer microchannel to enhance the strong vertical component of the Rayleigh wave, combined with tapered or fanned IDTs-based FACS, whose resonant frequency was in the range of 161–171 MHz. The device can sort cells at a rate of 9 kHz with 60% purity and yields of 92% purity at 1 kHz, which approaches the level of a FACS instrument.

3.1.2 Separation of other bioparticles. Similar to cells, if the difference in the size between the target bioparticles and heterogeneous populations is not significant, the biomarker-based sorting or fluorescence activated system will be applied. Liu *et al.*[57] made the use of carboxy-functionalized polystyrene (PS) microspheres conjugated with monoclonal anti-JEV antibody (mAb) to capture the Japanese encephalitis virus (JEV) in a complex biological sample (Fig. 4a). Then, TSAW of 46.1 MHz pushed the composites of PS-mAb-JEV out of the samples to achieve virus screening for further detection. The Korean group led by Yoon and Sung published papers on the separation of thrombin,[58] tardigrades,[59] and proteins of three kinds[60] successively. Aptamer15 (single-stranded DNA) labelled at one end with a biotin molecule, conjugated with streptavidin-functionalized PS microparticles *via* streptavidin-biotin linkage, was used to capture the target protein thrombin (th). The PS-apt15-th complex was separated from mCardinal2 and human serum using the high frequency of the 129 MHz TSAW device.[58] On this basis, this group used another different size of streptavidin-functionalized PS microparticles, conjugated with aptamerD17.4 labelled with a respective biotin molecule at one end, to capture the protein immunoglobulin E (IgE). The PS-apt15-th and PS-aptD17.4-IgE were separated simultaneously from mCardinal2 *via* a TSAW of 117 MHz (ref. 60) (Fig. 4b). In another work, to isolate tardigrades from raw samples, a passive microfluidic filter composed of an array of traps and a TSAW-based active (72 MHz) microfluidic device were implemented in turn. After the large algal clusters were removed, tardigrades were deflected from their original streamlines and then sorted out from algae and eggs, with a recovery of 96% and impurity of 4% algae on average.[59]

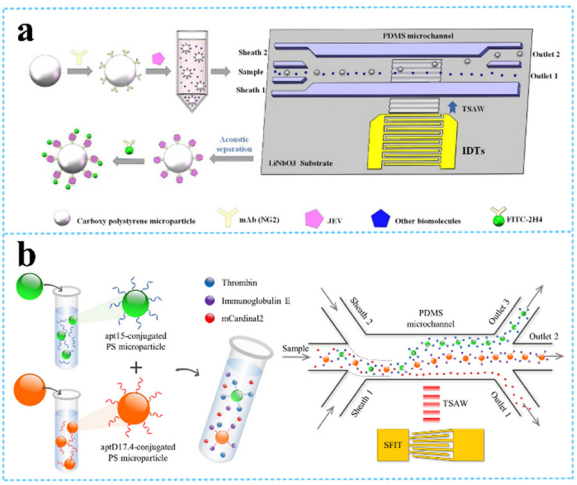

Fig. 4 TSAW devices for virus and protein separation. a: Schematic of JEV isolation and detection based on acoustofluidic driving and fluorescent labelling (reproduced from ref. 57 with permission from Elsevier, copyright 2020); b: schematic of the process for acoustofluidic triseparation of proteins (reproduced from ref. 60 with permission from American Chemical Society, copyright 2021).

3.2 SSAW-based separation

Two opposite traveling SAWs excited by two opposite IDTs form fixed pressure nodes and antinodes in an open or confined domain, often resulting in particles migrating toward acoustic nodes or antinodes. The acoustic contrast factor affects the particle motion, depending on the density and compressibility of the particles. Therefore, cells and solid particles will move toward the pressure nodes with positive acoustic contrast factor,[61] and lipids and gas bubbles will be pushed to the pressure antinodes with a negative acoustic contrast factor. The distance between the two nodes or two antinodes is half the wavelength. The wavelength can be designed to change the position of the nodes and antinodes to optimize the efficiency of separation.

3.2.1 Separation of cells. Usually, since particles of different sizes are subject to different acoustic radiation forces and the length of migration varies, through the continuous propulsion of fluid and SSAW, the sorting of particles is achieved. Nam *et al.*[62] employed a 7.54 MHz SSAW device to directly separate platelets from undiluted whole blood with a higher purity of nearly 98% than other methods (Fig. 5a). All blood cells, including red blood cells (RBCs), white blood cells (WBCs), and platelets, tended to be trapped in the pressure nodes for their positive acoustic contrast factor. However, platelets were mainly sorted in the center outlet because RBCs and WBCs were larger to be more efficiently driven to the side of the microchannel. Ai *et al.*[63] realized the efficient separation of *E. coli* bacteria from peripheral blood mononuclear cell (PBMC) samples with purity of 95%. The resonant frequency of SSAW was about 12.98 MHz and the pressure nodes were designed to be close to the side of the channel. Simon *et al.*[64] developed the bandpass sorting method, where a middle-sized particle was selected in two steps (Fig. 5b). In the first step, the larger-sized particles were separated from the smallest ones. Then, in the second step, by adjusting the frequency difference between two IDTs, the largest particles were pushed back with the smallest ones, leaving the middle-sized ones at the sorting node.

When the pressure nodal lines induced by SSAW are inclined at a specific angle to the flow direction, rather than being parallel to each other, the particles will move along the pressure nodal lines. As a result, the migration distance of

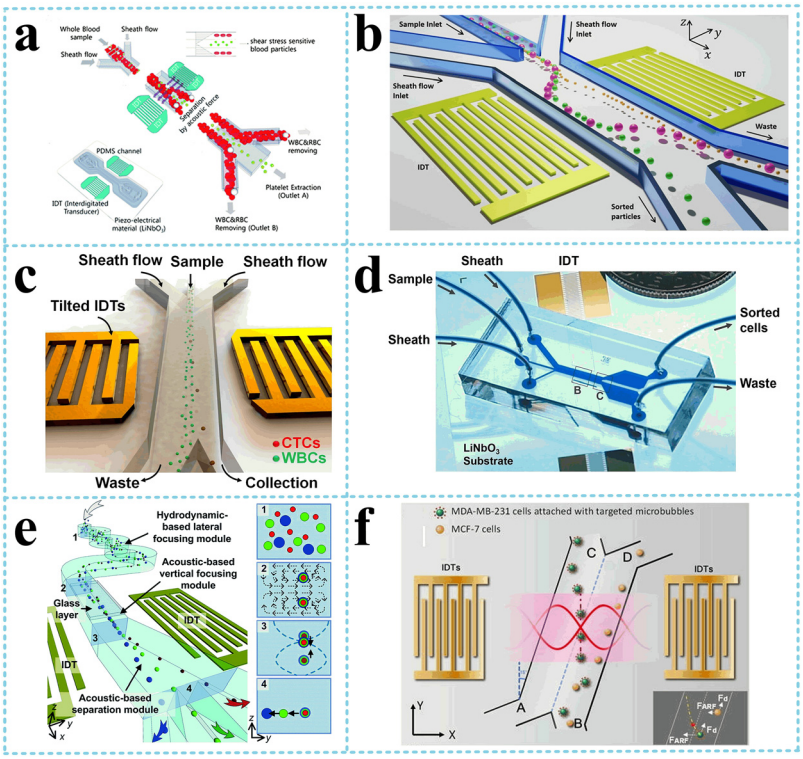

Fig. 5 SSAW devices for cells separation. a: Schematic image of the acoustic device with a pair of IDTs for selective platelet separation from whole blood (reproduced from ref. 62 with permission from the Royal Society of Chemistry, copyright © 2011); b: schematic of the bandpass acoustofluidic device for the separation of red blood cells from white blood cells;[64] c: schematic illustration and image of the high-throughput taSSAW device for cancer cell separation;[66] d: photo showing a taSSAW-based cell-separation device for sorting MCF-7 human breast cancer cells from nonmalignant leukocytes;[65] e: illustration of the 3D-AFT separation device for the separation of erythrocytes, leukocytes, and cancer cells (reproduced from ref. 67 with permission from the Royal Society of Chemistry, copyright 2018); f: schematic diagram of specific acoustic tweezers for the isolation of MDA-MB-231 from MCF-7 cells (reproduced from ref. 69 with permission from AIP Publishing, copyright 2020).

the particle along the direction perpendicular to the flow could be a few times or tens times the acoustic wavelength, depending on the geometry of the channel, which is significantly higher than that of the conventional acoustic separation approaches. In addition, there are multiple pressure nodal lines instead of only one in the traditional SSAW separation methods, meaning that the target particles can be trapped again on escaping. Based on this principle, Ding *et al.*[65] and Li *et al.*[66] employed tilted-angle SSAW (taSSAW) devices, isolating CTCs in blood samples and sorting MCF-7 human breast cancer cells from nonmalignant leukocytes, respectively (Fig. 5c and d). Wu *et al.*[67] designed a complex microchannel with three specific functions (Fig. 5e). After the particles aligned in a single line by hydrodynamic-based lateral focusing module and acoustic-based vertical focusing module, the third module with titled and widening microchannel separated particles by size and density. They successfully sorted out leukocytes from erythrocytes and cancer cells from leukocytes.

Particles with different acoustic contrast factors also receive different acoustic radiation force, determined by density and compressibility. Xie *et al.*[68] separated paraformaldehyde-treated and fresh HeLa cells based on the differences in the mechanical properties with a recovery rate of 85% for fixed cells and also separated RBCs and WBCs, which had different densities with a recovery rate of 80.5% for WBCs *via* a SSAW device with an operating frequency of 12.89 MHz. As mentioned above, bubbles have negative acoustic contrast factor opposite to the cells. By attaching the targeted microbubbles to MDA-MB-231 cells, Meng *et al.*[69] separated MDA-MB-231 from MCF-7 cells, two kinds of cells with an overlap in size distribution, with an efficiency of 91.2%, using tilted IDTs generating an SSAW of 11.4 MHz (Fig. 5f).

To improve the efficiency and expand the applications of SSAW in biological separation, many advanced technologies are integrated. Hu *et al.*[70] applied acoustic and optical technologies together to isolate precisely three main types of leukocyte subtypes. The former was used to separate granulocytes, which had evident size distinction from other components, and the latter can distinguish lymphocytes and monocytes, which have an overlap in size or density, *via* RI difference. Nawaz *et al.*[71] combined real-time fluorescence and deformability cytometry with SSAW to transfer molecular specificity to image-based sorting using an efficient deep neural network, establishing a sorting platform based on cell functional changes; Pei *et al.*[72] utilized a compact driver based on current feedback amplifiers to drive IDTs, which

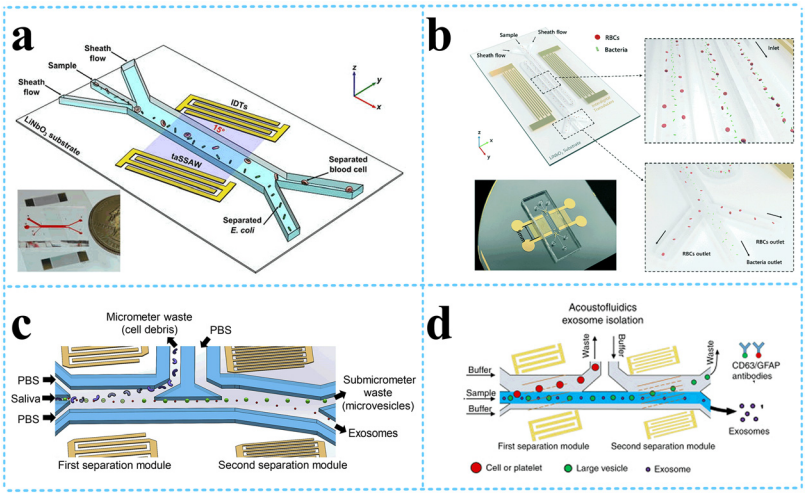

Fig. 6 SSAW devices for other bioparticle separation. a: Schematic of acoustofluidic separation of *E. coli* from human blood samples using the taSSAW technique (reproduced from ref. 74 with permission from IOP Publishing, copyright 2017); b: the SSAW-enabled serpentine microfluidic device for high-throughput bacterial separation from human blood cells (reproduced from ref. 75 with permission from the Royal Society of Chemistry, copyright 2021); c: schematic of the acoustofluidic device for salivary exosome separation (reproduced from ref. 79 with permission from American Society for Investigative Pathology and the Association for Molecular Pathology, copyright 2020); d: schematic detailing the process of exosomes isolation from plasma samples.[80]

can drive a wider range of loads without impedance matching and significantly reduced the power consumption by working in a switch mode triggered by target cells.

3.2.2 Separation of other bioparticles. Ai *et al.*[73] separated *Escherichia coli* bacteria premixed in PBMCs by SSAW (13 MHz) at a purity of 95.65% based on the size difference. Li *et al.*[74] employed a taSSAW device to sort out *Escherichia coli* from human blood cells with a purity of more than 96% (Fig. 6a). Ning *et al.*[75] applied a serpentine microchannel to multiply the operating distance of the SSAWs *via* the "spatial multiplexing" and "pressure node matching", realizing high-throughput separation of bacteria from human blood cells (Fig. 6b). For other smaller bioparticles, the sorting can be achieved by pushing the larger particles out as waste. Lee *et al.*[76] utilized a SSAW device as a nanofilter to isolate nanoscale (<200 nm) vesicles from cell culture media as well as MVs in stored red blood cell products. To decrease the critical diameter when particles can be pushed, Tayebi *et al.*[77] combined dielectrophoretic (DEP) and acoustophoretic force. Exosomes (<200 nm) and microvesicles (>300 nm) were sorted out with more than 95% purity and 81% recovery.

Exosomes are nanovesicles with a diameter of 30–150 nm, carrying nucleic acids, proteins, lipids, and other molecules from their cells of origin. Exosomes can be found in nearly all biological fluids, including blood, saliva, urine, semen, sputum, breast milk, and cerebrospinal fluid; thus, they can be collected noninvasively to continuously monitor the disease progression. Thus, the separation of exosomes has attracted great interests from researchers. The group from Duke University designed an acoustofluidic separation chip containing two pairs of IDTs generating taSSAWs. They utilized this kind of chip to isolate exosomes from whole blood by removing larger cells and vesicles in turn,[78] exosomes from saliva samples[79] o detect human papillomavirus (HPV) DNA in exosomes (Fig. 6c), exosomes from plasma samples to detect exosomal biomarkers for traumatic brain injury (TBI) *via* flow cytometry[80] (Fig. 6d), and also to sort out and purify the nanometer Alzheimer's disease (AD) biomarkers (proteins, exosomes, *etc.*), which can be used for early diagnosis of AD.[81]

4. Real-time biosensors based on SH-SAW

The wave velocity of the acoustic wave and the direction of the particle motion on the surface determine whether the device can be used in liquid detection. If the particle motion is perpendicular to the surface of the device and the wave velocity is larger than the compressional wave velocity in the liquid, the acoustic energy will be scattered into the liquid as a compressional wave (compressional or longitudinal), resulting in significant attenuation.[82] As the particle displacement of the Rayleigh wave has only two components, one is the tangential component along the propagation direction parallel to the surface, it will be viscous with the liquid medium, and there is no component normal to the interface, which will not cause vibration in the liquid. The other is the longitudinal component perpendicular to the surface, which in the liquid medium will produce the corresponding compression wave, acoustic energy radiation into the liquid layer, causing acoustic attenuation. Therefore, to enable the use of SAW devices as liquid sensors, it is necessary to excite the horizontal displacement component and suppress the longitudinal component. The commonly used piezoelectric materials do not meet this requirement and are unable to obtain acoustic signals in liquids. SH-SAW

solves this problem very well because during the propagation of SH-SAW, the vibration direction of the solid surface mass is parallel to the surface of the piezoelectric substrate and perpendicular to the propagation direction of the acoustic wave; thus, the acoustic wave energy will not be lost to the liquid during the propagation process.[83]

SH-SAW sensor structures are usually divided into two types: delay-line and resonant. Resonant sensors are usually used for physical sensing such as stress and temperature because they consist of IDTs and metal reflective grids on both sides, which cannot operate directly in liquid phase conditions. Therefore, delayed-line sensors are chosen for biochemical detection applications. Delay-line sensors consist of transmitter IDTs, receiver IDTs, and an intermediate delay line. Since the biosensor operates in a liquid phase environment, the delay line structure can provide a response zone for the bioassay. The structure of the SH-SAW biosensor device is shown in Fig. 7,[84] where the motor-to-electric signal conversion is achieved by loading the input IDTs with AC signals of specific frequencies, and the SAW device generates and detects acoustic waves through the IDTs on the piezoelectric substrate.[85] During bioassays, analyte-specific molecules (*e.g.*, antibodies) are immobilized on the SAW device to capture analyte molecules (*e.g.*, antigens) from the sample stream. When the two are combined, their mass loading changes, which will cause the phase amplitude and speed of the SAW to change, thus affecting the output electrical signal.[86]

The operating principle of the device is similar to that of a Rayleigh wave device. The acoustic surface waves are generated by the excitation of the input IDTs on the piezoelectric substrate, and subsequently, the IDTs detection signal can be output. The main difference between the Rayleigh wave device and this device is the direction of acoustic particle vibration, and the piezoelectric substrate material is the most significant factor contributing to this result. The typical operating frequency of the device is 30–500 MHz, and the sensitivity is 100–180 $cm^2\ g^{-1}$. The most commonly used substrate material for the device is 36° YX lithium tantalate, while other materials such as ST-cut quartz, 41° YX lithium niobate, 64° YX lithium niobate, and potassium niobate have also been reported as piezoelectric substrates for SH-SAW devices. The dielectric constant ε is an important parameter in the selection of piezoelectric substrate materials. If the sensor operates in an aqueous solution, the dielectric constant of the material should be close to that of water (ε ≈ 80) to reduce the capacitive effect at DTs, *e.g.*, using lithium tantalate (ε = 47).

SH-SAW is suitable for liquid sensing because only the elastic wave vibrating in the horizontal shear direction exists, and the energy radiated into the liquid is small. In addition, SH-SAW for liquid sensing has the following advantages:[87] 1) the structure of the SH-SAW sensor is similar to that of the Rayleigh wave sensor, which can be made into a high frequency sensor; 2) the sensor size is small, which is convenient for the micro measurement of specimens and miniaturization design of the detection system; 3) the measurement speed is fast, which is convenient for real-time monitoring.

4.1 Detection of biomolecules

Onen *et al.*[88] successfully designed and fabricated a urinary anti-apoptotic protein B-cell lymphoma 2 (Bcl-2) SAW biosensor for early ovarian cancer detection using multiple materials for optimization of the formulation to achieve the most efficient Bcl-2 capture (Fig. 8a). By placing a known concentration (in DPBS) of Bcl-2 buffer solution in the delay path, the increased mass loading of biomarker binding caused a resonant frequency shift, which reduced the velocity of SH-SAWs. The sensor was able to successfully detect Bcl-2 in the concentration range of 0.5 to 12 ng mL^{-1}, which has potential applications in the diagnosis and quantification of ovarian cancer. In addition to this, it was found that each sensor was used up to 10 times with no change in the sensitivity, achieving a certain degree of device reusability. C-reactive protein (CRP) is an acute positive marker of inflammation and is widely used for diagnostic purposes. Pomowski *et al.*[89] coated SH-SAW with 2-methacryloyloxyethyl phosphorylcholine (MPC) polymer for the label-free detection

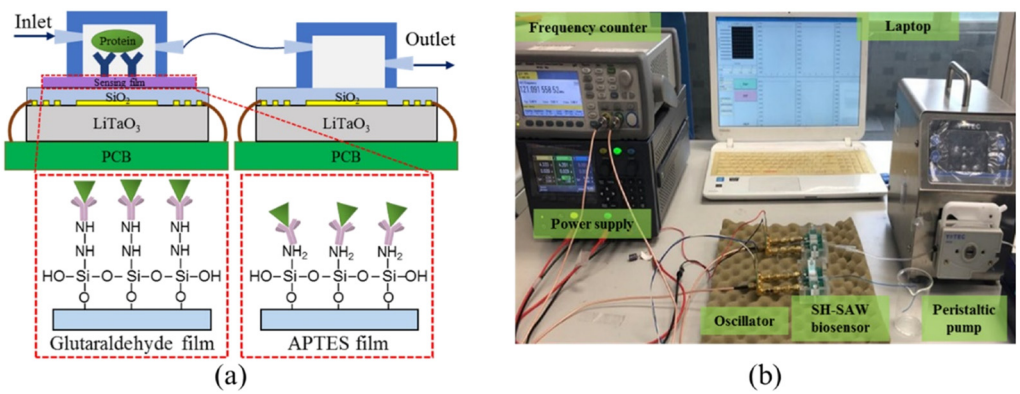

Fig. 7 Schematic of the SH-SAW biosensor device. a: Configurations of the dual SH-SAW biosensors and the illustration of EGF antigen binding on these two films; b: experimental apparatus.[84]

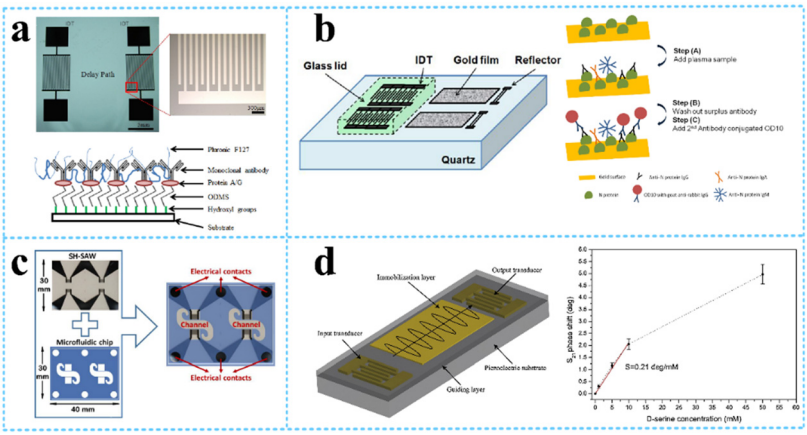

Fig. 8 SH-SAW devices for biomolecule detection. a: fabricated SH-SAW biosensor for urinary anti-apoptotic protein Bcl-2 detection and illustration of surface functionalization;[88] b: schematic of SH-SAW sensor chip and measurement protocol for anti-N protein IgG detection;[90] c: a system of SH-SAW immunosensor combined with a microfluidic chip for the detection of FGF-2;[93] d: schematic representation of the SH-SAW delay-line and response curve of SAW biosensor at different concentrations of D-serine (reproduced from ref. 94 with permission from Elsevier, copyright 2016).

of the inflammatory marker C-reactive protein (CRP) in human serum. This method both binds CRP and reduces the nonspecific adsorption of other proteins, thus allowing differentiation between human CRP serum concentrations in the normal range (10 mg L^{-1} and below) and those indicating bacterial infection. An SH-SAW biosensor was also developed for the detection of anti-SARS-CoV-2 capsid antibodies, which achieved high correlation coefficients (R = 0.9997) at different concentrations (34.375–1100 ng mL^{-1}) of "spiky" anti-N protein antibodies, with better sensitivity compared to ELISA (Fig. 8b). The SH-SAW biosensor proved to be a promising platform for rapid *in vitro* diagnostic (IVD) testing.[90]

Trivedi *et al.*[91] presented a high-sensitivity SH-SAW resonator using SiO_2 trenches and mass loading of the device with DNA, producing a large frequency shift of more than 5 MHz under coupled resonance conditions, which was 10 times larger than that obtained under uncoupled resonance conditions. It has high sensitivity for DNA detection. The immobilization of a 27-mer DNA-probes on the SH-SAW gold sensitive layer and subsequent hybridization with 36-mer complementary DNA-targets were investigated. The mass sensitivity deduced from immobilization frequency curves was 6.3 Hz ng^{-1}.[92] SH-SAW could also be used to identify the growth factors in real time. Growth factors (GFs) are biomolecules involved in various cellular processes, and the dysregulation of GFs signalling can lead to various diseases. The sensor could detect FGF-2 growth factors in the concentration range of 1–25 μg mL^{-1} with a total test time of 15 min and an LOD of 130 ng mL^{-1}. This was due to an increase in the mass due to antibody–antigen affinity, which produced a change in the surface acoustic wave rate and therefore a change in the resonant frequency (Fig. 8c).[93] Since D-amino acid levels are often associated with different neurological disorders, it is important to develop rapid and specific biosensors for the determination of D-serine. Pietrantonio *et al.*[94] fabricated a SAW biosensor with a PLP-reduced D-serine dehydratase for the detection of D-serine levels (Fig. 8d). In the experiment, this enzyme was able to bind D-serine and did not bind other substances, indicating that the biosensor has high specificity and selectivity for D-serine. The effect of D-serine concentration on the displacement variation was also explored, and a linear variation was found over the concentration range between 0.0 mM and 10 mM with a sensitivity of S = 0.21 deg mM^{-1}. In addition to this, the SAW biosensor response remained sensitive after extensive washing steps on the gold wafer.

4.2 Detection of cells

The SH-SAW-based biosensor allowed the analysis of the degree of wound healing by observing cell growth and quantifying the cell detachment process (Fig. 9a). Primarily, epithelial cells were cultured on a substrate and invade the sensor, resulting in a phase shift of the transmitted SAW signal, and the signal slope could quantify the cell detachment process induced by apoptosis, necrosis, or cell lysis, respectively. In addition, the SAW sensor could monitor culture conditions such as temperature or osmotic pressure. Thus, the SAW sensor achieved the ability to analyze the extent of wound healing without microscopic observation.[95] The effect of H_2O_2 (0.5 and 1.0 mM) on cellular tissue function, particularly transepithelial resistance and paracellular permeability, under the same conditions was investigated by attaching cultured cells to a cell adhesion matrix of the SH-SAW device, and the loss and phase shift of the SH-SAW signal was observed in the open channel.[96]

The 2014 Ebola outbreak was the largest in history, and the early detection of this highly infectious virus will help improve infection control measures. The SH-SAW platform could obtain phase shifts by continuously measuring the difference between the reference signal and the Ebola signal and could detect target antigens in various types of media,

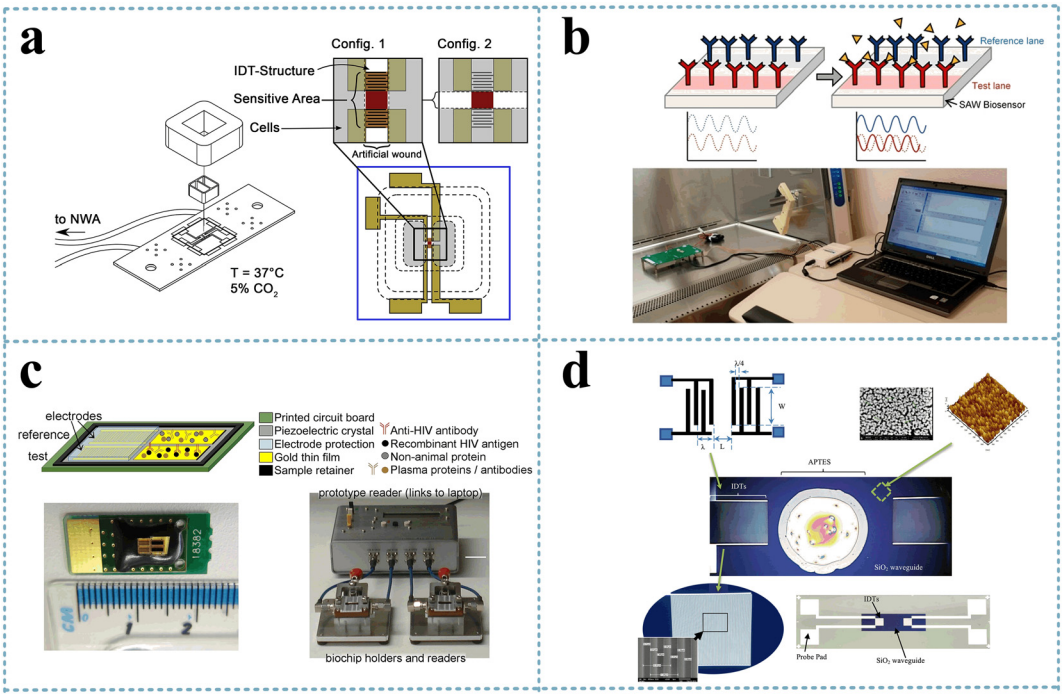

Fig. 9 SH-SAW devices for cell detection. a: Schematic of the experimental setup and the SAW-chip for the assessment of the migration rate of epithelial cells (reproduced from ref. 95 with permission from Elsevier, copyright 2021); b: schematic of a SAW biosensor and detection system for the rapid detection of Ebola virus;[97] c: SH-SAW biosensor and biochip for the detection of HIV infection;[98] d: SH-SAW biosensor with SiO_2 nanoparticles waveguide for the detection of *E. coli* (reproduced from ref. 100 with permission from Elsevier, copyright 2017).

reaching detection limits of <50 pg cm^{-2}, with fast virus detection (within 2 min) (Fig. 9b).[97] HIV is easily transmitted, and early diagnosis would facilitate the control of its spread. A dual-channel SH-SAW biochip was designed to detect antibody markers of HIV infection with an *in situ* reference control coating and a miniaturized configuration that requires only 6 μL of plasma for detection (Fig. 9c). With sensitivities of 100% (anti-gp41) and 64.5% (anti-p24) within 5 min, it exhibited excellent sensitivity, specificity, low sample volume, and rapidity.[98] An SH-SAW device biosensors was fabricated on rhodochrosite (LGS) Euler angles (0°, 22°, 90°) for the detection of *E. coli* O157:H7 using liquid phase flow-through and dip-dry methods for the experiments. LGS SH-SAW delay lines were prepared and derivatized with a rabbit polyclonal IgG antibody, which selectively bound to *E. coli* O157:H7. The phase of the biosensor transmission coefficient was monitored by suspending the tested *E. coli* in phosphate buffered saline and applying it to the antibody-coated sensing surface. The phase response for *E. coli* detection measured approximately 14° compared to 2° for non-specific anti-TNP binding, demonstrating its potential application for bacterial detection.[99] An SH-SAW biosensor with silica nanostructured waveguides for the detection of *E. coli* O157:H7 was also presented (Fig. 9(d)). The sensor was specific for *Escherichia* O157:H7 oligonucleotide targets and could analyze the frequency shift in response to different concentrations of oligonucleotides with a sensitivity of 0.6439 nM/0.1 kHz and a detection limit as low as 1.8 fM (1.8×10^{-15} M).[100]

5. High sensitivity biosensors based on LW-SAW

As described earlier, the sensitivity of the SH-SAW devices is often enhanced using a thin guiding layer. The

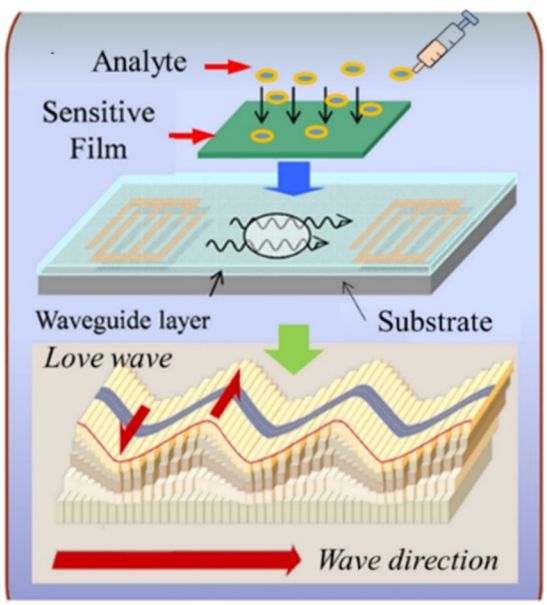

Fig. 10 Schematic of the Love waves and the basic structure of an LW-SAW sensor (reproduced from ref. 105 with permission Elsevier, copyright 2018).

waveguiding occurs when the shear wave velocity in the guiding layer is less than the velocity in the substrate with an appropriate thick guiding layer. This type of horizontally polarized shear SAW is named the Love wave after Augustus Love who predicted their existence in 1911.[101] As shown in Fig. 10, for a LW-SAW to exist, there needs to be a finite thick layer over a semi-infinite substrate, and the shear horizontal bulk wave velocity in the layer must be less than that in the substrate material. When this happens, the layer slows down the acoustic shear mode in the substrate so that the penetration depth is decreased and the acoustic energy is confined to the surface.[102] Thus, the LW-SAW can be described as a high-frequency SH-SAW with a guiding layer that contains and maintains the wave energy to the surface while reducing the wave propagation velocity.[103]

The LW-SAW device is a layered structure basically consisting of a thick piezoelectric substrate and a thin guiding layer on the top of the substrate.[104,105] Substrates such as silicon, quartz, $LiTaO_3$, and $LiNbO_3$ are usually employed for LW-SAW, while various materials such as SiO_2, ZnO, TiO_2, PMMA, and SU-8 photoresist are deposited on top of the substrates as the waveguiding layers.[106] The piezoelectric substrate of a LW-SAW device primarily excites a shear horizontal surface acoustic wave (SH-SAW). Due to the horizontal polarization, LW-SAW does not couple with liquids and is compatible with measurements in liquids. Apart from keeping the wave's energy to the surface while reducing the velocity of wave propagation, the waveguiding layer can also act as an additional protection against harsh liquid environments.[107]

The operating principle of the LW-SAW device is basically the same as the SH-SAW sensors. The waves generated from the emitter propagate through the delay line area to reach the receptor part, where it is further converted into the corresponding electrical pulse. Any changes in the delay line area as a result of chemical/biological reactions will be reflected by the output electrical pulse since such perturbations can change the propagation velocities of the SAW. During the biosensing process, the adsorption of biomolecules on the delay line area may result in a mass increase in the device surface, ultimately altering the center frequency of the SAW device. The intensity of the change is considered as corresponding to the extent of mass deposition on the delay line area and can be determined by a suitable oscillator circuit. Therefore, a suitably prepared bioreceptor on the delay line area of the SAW device can be used as a selective and sensitive layer for the sensing of various biomolecules. On account of the high sensitivity and capacity for gas and liquid detection, LW-SAW devices have been exploited as sensors for the detection of various biological objectives such as proteins,[108–110] nucleic acids,[111,112] organic molecules,[113–115] cells,[116–118] and microorganisms.[119–121]

5.1 Detection of biomolecules

LW-SAW sensors have been developed for the detection of various biomolecules including proteins, nucleic acids, and organic molecules. Numerous early attempts[109,122–125] have been focused on IgG detection since Gizeli *et al.*[122] firstly reported a polymer-coated Love plate device. The device consisted of Y-cut quartz substrate and PMMA waveguiding layer at a frequency of 110 MHz was performed to detect IgG in the range of 1–400 μg mL^{-1}. Oh[109] developed a LW-SAW based wireless immunosensor with a 440 MHz operating frequency, which was composed of a shear horizontal surface acoustic wave (SH SAW) reflective delay line, a PMMA waveguide layer, and a 2,4-dinitrophenyl (DNP) receptor layer that specifically responds to an anti-DNP immunoglobulin G (IgG). Due to the affinity of different IgG concentrations to the DNP-bound gold surface, a fast response time (3 min), a large phase shift (2700 phase shift for 0.2 mg mL^{-1} IgG solution), and high testing stability were observed by the developed LW-SAW sensor. Tretjakov[125] applied molecularly imprinted polymer (MIP)-based synthetic receptors integrated with the LW-SAW sensing platform for the first time for label-free protein detection (Fig. 11a). The ultrathin polymeric films with surface imprints of immunoglobulin G (IgG-MIP) were fabricated onto the multiplexed SAW chips using an electrosynthesis approach. The prepared IgG-MIPs demonstrated good selectivity toward IgG over the interfering proteins such as IgA and HAS. The facile integration of the protein-MIP sensing layer with SAW technology allowed the observation of the real-time binding events of the target protein at relevant sensitivity levels and can be potentially suitable for the cost-effective fabrication of a biosensor for the analysis of biological samples in a multiplexed manner.

In recent years, more and more LW-SAW devices have been used for the early identification of cancers, which are based on the detection and estimation of tumor marking proteins in body fluids, such as carcinoembryonic antigen (CEA),[110,126–130] neuron specific enolase (NSE),[110] squamous cell carcinoma antigen (SCC),[110] tumor necrosis factor-α (TNF-α),[131] and prostate-specific membrane antigen (PSMA).[132] Zou *et al.*[110] presented a sensitive LW-SAW immunosensor that provided the rapid, sensitive, specific, and accurate detection of CEA, NSE, and SCC in exhaled breath condensate for the early diagnosis of lung cancer. The immunosensor was based on ST-cut quartz substrate and SiO_2 guiding layer with a frequency of 165 MHz and utilized immune gold staining as a signal enhancement method. The LOD was estimated to be 0.967 ng mL^{-1}, 1.598 ng mL^{-1}, and 0.663 ng mL^{-1} for CEA, NSE, and SCC, respectively, which was much lower than the corresponding cut off values to distinguish patients with lung cancer and healthy subjects. Later, Fu and his colleagues continuously developed several LW-SAW biosensors for CEA detection based on ST-cut quartz and different guiding layers including negative UV photoresist (SU-8),[128] polyimide (PI),[129] and SiO_2.[130] They

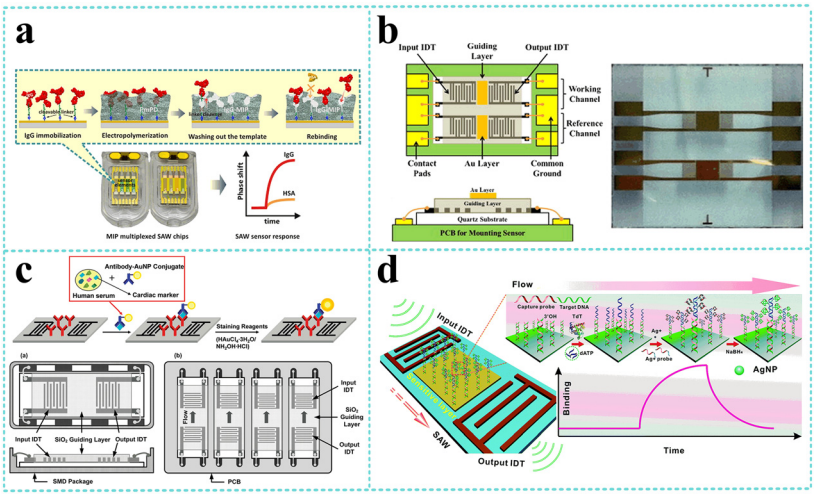

Fig. 11 LW-SAW devices for biomolecule detection. a: Schematic of the synthesis concept for IgG-MIP sensing layer integration with SAW chip (reproduced from ref. 125 with permission from Elsevier, copyright 2016); b: schematic of the LW-SAW sensor chip for CEA detection in exhaled breath condensate (reproduced from ref. 126 with permission from Elsevier, copyright 2015); c: schematic of the sandwich immunoassay format and LW-SAW sensor array for cardiac markers detection (reproduced from ref. 133 with permission from American Chemical Society, copyright 2011); d: schematic illustration of an SAW biosensor for highly specific and signal-amplified DNA detection (reproduced from ref. 111 with permission from the Royal Society of Chemistry, copyright 2017).

immobilized CEA antibody on the SAW delay line by different strategies such as Au coating, PI/AuNP-MoS_2-rGO thin film, or AuNPs coating through the thioglycolic acid–EDC/NHS reaction mechanism. These attempts significantly amplified the mass loading effect and reduced the LOD to as low as 0.084 ng mL^{-1}.

Cardiac markers, which play an essential role in the diagnosis, prognosis, monitoring, and risk stratification of suspected heart attack patients, have also attracted great attention from researchers in the field of LW-SAW biosensors. Lee *et al.*[133] presented a highly sensitive 200 MHz Love wave SAW biosensor that can achieve individual and simultaneous detection of multiple cardiac markers (myoglobin, CK-MB, and cTnI) in human serum below clinical cut off levels (Fig. 11c). To improve the detection limit, a 400 MHz sensor chip was designed to investigate the effects of increasing operating frequency on the sensor response. Compared with the 200 MHz sensor chip, it produced approximately 2 times higher slope of frequency response *versus* cTnI concentration in the range of 0.02–50 ng mL^{-1}. These results highlight the potential that the detection limit of the SAW sensor can be further improved by increasing the operating frequency with accompanying noise level and stability taken into account. Mitsakakis *et al.*[134] reported a 155 MHz LW-SAW sensor with a polymethylmethacrylate (PMMA) guiding layer for the rapid and efficient analysis of multiple cardiac markers, including creatine kinase MB (CK-MB), cardiac reactive protein (CRP), D-dimer, and pregnancy-associated plasma protein A (PAPP-A). The presented multi-analyte acoustic biosensing platform, which can be operated to detect four biomarkers in complex analyte samples in less than 30 min, has great potential as a reliable diagnostic tool for cardiovascular diseases.

In addition to proteins, nucleic acids and organic molecules (such as uric acid,[114] glucose,[113,135] and dopamine[115]) are also able to be detected by LW-SAW sensors. Zhang *et al.*[111] reported a surface acoustic wave (SAW) DNA sensor that synergizes the surface mass effect for signal-amplified and sequence-specific DNA detection in blood serum (Fig. 11d). By combining an enzyme-mediated DNA extension reaction (both viscoelastic and mass fractions) with the *in situ* synthesis of silver nanoparticles (mass fraction), the sensor improved the detection limit (0.8 pM) by 3 orders of magnitude as compared to the strategy without signal amplification (at the nanomolar level). Han *et al.*[115] electrodeposited a ternary hybrid material composed of Ni nanoparticles (NPs), TiO_2 NPs, and poly(L-lysine) (Ply) onto the sensing area of a commercial 433 MHz SAW resonator to fabricate a LW-SAW sensor to detect the dopamine level in serum. The LW-SAW biosensor responded to DA with a linear concentration range from 1 to 1000 nM and limit of detection of 0.067 nM.

5.2 Detection of cells

Molecular interactions that govern cell–cell and cell–substrate communication is of great importance in biology. Assays that employ whole cells and focus on the interactions that drive a particular biological process in a non-invasive way are particularly useful. Acoustic biosensors can be extremely advantageous for studying events such as cell adhesion and motility since they respond not only to net mass changes but also to differences in the physiological conditions of cells or cell layers.[136] Saitakis *et al.*[116] employed a LW-SAW device and a quartz crystal microbalance system with dissipation (QCM-D) to demonstrate the potential of acoustic devices to

probe the binding of a cell membrane receptor to an immobilized ligand. The probed HLA/anti-HLA binding pair was chosen as a model system to mimic the function of this cell membrane molecule that mediates cell–cell intercommunication. Compared with a SPR sensor that was indiscriminate of specific or non-specific binding, QCM-D and LW-SAW could detect the molecular interaction between the immobilized antibody and HLA. Bröker *et al.*[117] developed a nanostructured LW-SAW chip that could detect extremely low numbers of circulating tumor cells (CTC) without labelling by defining the interspacing between tumor cell surface-specific antibodies. JEG-3 and MOLT-17 cells were successfully detected at extremely high sensitivity. The sensor showed significant response to less than 10 cells injected in a single run. Compared with a complete gold surface, the sensitivity was increased by more than 100-fold at unchanged high selectivity. Wu *et al.*[118] adopted a 36° YX-$LiTaO_3$-based LW-SAW sensor with a parylene-C waveguiding layer as a cell-based biosensor to monitor the adhesion process of tendon stem/progenitor cells (TSCs). The LW-SAW sensor exhibited high sensitivity to surface perturbations, especially bonds formed within the relatively short distance from the surface, indicating their potential for investigating subtle interactions between cell membranes and substrates involved in a variety of cellular activities. The sensor response to the adhesion process of TSCs exhibits high consistency with the experimental observations, providing a recommended method to investigate a series of cellular activities.

Virus detection by LW-SAW devices for the diagnosis of viral infectious diseases are generally approached by the quantitative determination of viral cell surface antigens. Lee *et al.*[121] demonstrate the application of the LW-SAW immunosensor to detect hepatitis B surface antibody (HBsAb) in whole blood samples without any pretreatment. The mass sensitivity was found to be 0.74 Hz/(pg/μl), and the detection limit was below 10 IU L^{-1}, which is the protective HbsAb level. In addition, the lack of additional equipments and expensive reagents, such as fluorescence labelling probes with short shelf lives, allows the system to be portable and commercially viable. Jiang *et al.*[119] presented a LW-SAW sensor for influenza A viral antigen detection, which could capture the target analyte selectively through the antigen and antibody interaction enabled with appropriate surface functionalization (Fig. 12a). The detection limit of influenza A HAH1N1 antigen at an analyte concentration as low as 1 ng mL^{-1} was demonstrated without any compensation design at room temperature with the LW-SAW sensors.

Various food pathogenic bacteria such as *Staphylococcus aureus* (*S. aureus*), *S. typhimurium*, *B. cereus*, *Listeria*, and *Escherichia coli* (*E. coli*) have a strong potential to cause food poisoning and can cause localized purulent infection, pseudomembranous colitis, pneumonia, and even some systemic infections.[137] Xu and Yuan[120] compared the sensitivity of QCM, Rayleigh-SAW, and LW-SAW sensors for the quantification of *Staphylococcus aureus* (*S. aureus*). The ZnO nanoparticle-based LW-SAW sensor had a maximum mass loading sensitivity of 328.75 Hz ng^{-1} and achieved a lower limit of detection of 2×10^3 CFU mL^{-1} compared to the QCM counterpart under the same conditions. The LW-SAW sensor could be used as a disposable chip in micro or ultratrace accurate diagnosis methods. Tsougeni *et al.*[138] presented an integrated lab-on-chip (LoC) platform encompassing an optimized compact, plasma nanotextured chip for bacteria capture, lysis, and DNA amplification all in one chamber, integrated with a LW-SAW sensor for the detection of four different bacteria (*S. typhimurium*, *B. cereus*, *Listeria*, and *E. coli*) (Fig. 12b). The efficiency of the analysis

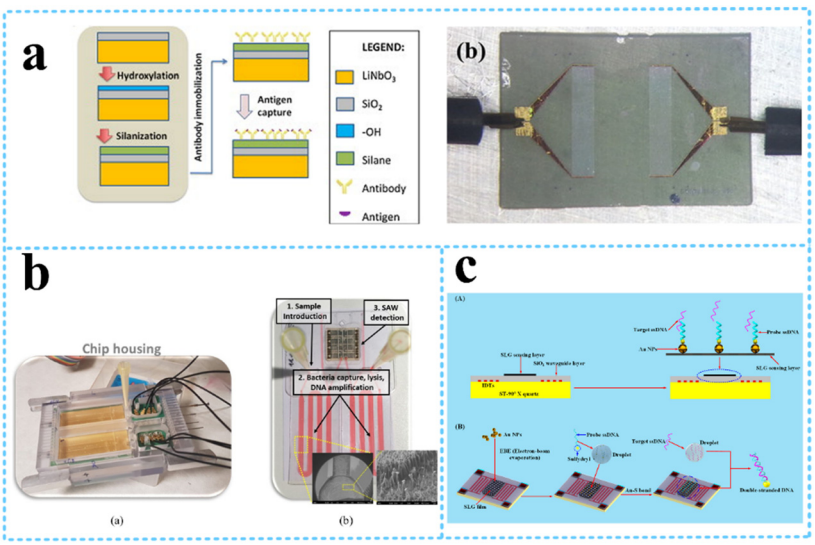

Fig. 12 LW-SAW devices for cell detection. a: Schematic of the LW-SAW sensor for influenza A viral antigen detection (reproduced from ref. 119 with permission from Elsevier, copyright 2015); b: bacteria (reproduced from ref. 138 with permission from Elsevier, copyright 2020); c: *S. aureus* gene sequences (reproduced from ref. 112 with permission from American Chemical Society, copyright 2020).

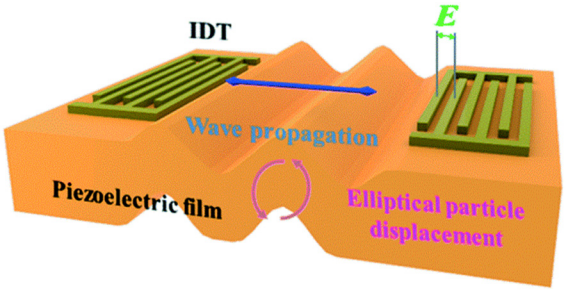

Fig. 13 Illustrations of the generation of Lamb wave (reproduced from ref. 140 with permission from the Royal Society of Chemistry, copyright 2020).

within the LoC platform was demonstrated for an initial concentration of 1–5 CFU mL^{-1} in 25 mL of whole milk and within 70 min. Ji *et al.*[112] reported a single-layered graphene (SLG)/Au-nanoparticles (NPs)-based LW-SAW biosensor for the detection of *S. aureus* gene sequences (Fig. 12c). The biosensor achieved a linear detection ranging from 0 to 10 nmol L^{-1} with an LOD of 12.4 pg mL^{-1}, and holds great potential in clinical testing and diagnosis.

6. Flexible SAW devices based on the Lamb wave

Lamb waves, which are generated when the substrate thickness is smaller than (or comparable to) the wavelength of the wave, are equivalent to Rayleigh waves in their thin plate-like substrates instead of the bulk substrates, as illustrated in Fig. 13. They can either be (i) passive Lamb waves without the use of a piezoelectric substrate, which are normally generated from a remote acoustic wave source; (ii) positive Lamb waves generated by a thin piezoelectric layer itself. Lamb wave devices are generally realized using very thin film piezoelectric films, such as zinc oxide (ZnO), aluminium nitride (AlN), and piezoelectric transducer (PZT), forming membrane-like devices with the thickness of the plate being only a small percentage of the acoustic wavelength. Typically, Lamb waves propagating in thin plates or membranes have two modes at low frequencies—the fundamental antisymmetric Lamb wave and symmetrical Lamb wave.[139]

The zero-order antisymmetric mode, A_0, which is often called flexural plate wave mode (FPW), is highly dispersive in the low frequency regime. At higher frequencies, the wave velocity converges toward the Rayleigh wave velocity. With increasing layer thickness, the A_0 wave gradually changes into the Rayleigh wave or a higher order *A*-mode wave. Once the thickness of the FPW device increases or the acoustic wave power increases, the A_0 mode can radiate wave energy into the surrounding medium, causing acoustic streaming parallel to the device surface. Therefore, the FPW modes have been proposed for mixing and pumping applications. The potential applications of acoustic streaming with the FPW include micro total analysis systems (μTAS), cell manipulating systems, and drug delivery systems. Luo's group has carried out a series of researches demonstrating flexible SAW devices on polyimide (PI), which can realize many microfluidic functions such as streaming, mixing, and particle concentration.[141,142] They fabricated flexible SAW resonators using ZnO nanocrystal deposited on a PI substrate, which had the Rayleigh wave and Lamb wave resonances. Strong acoustic streaming with a velocity of up to 3.4 cm s^{-1} and particle concentration using SAW have been achieved. The flexible devices have been tested for the ability to perform particle concentration and sorting functions.[141] Peng *et al.*[143] accomplished microparticle concentration within sessile droplets placed on the hydrophobic surface, which benefited from streaming flow induced by the Lamb wave propagated in the glass waveguide to manipulate particles in the droplets. Microparticles were concentrated at the central area of the droplet adhesion plane based on the balance among the streaming drag force, gravity, and buoyancy at the operating frequency, as shown in Fig. 14a. In addition, Wang *et al.*[144] provided a guide for the design and manufacture of flexible, efficient acoustofluidic devices, by systematically investigating acoustofluidic behaviors of ZnO/Al sheet SAWs and comparing the performance with those of conventional ZnO/Si SAWs, focusing on the thickness effects on the wave modes and microfluidic performance. In the example of Al sheets, a thickness of 200 μm enables optimal fluid transportations along various mechanically bent/deformed surfaces (Fig. 14b), paving the way for flexible/bendable or wearable applications. In a recent work, Duan *et al.*[145] presented a versatile acoustofluidic platform actuated by a Lamb wave resonator (LWR) array, in which pumping, mixing, fluidic switching, and particle trapping are all achieved on a single chip. The acoustofluidic platform was further tested for prostate specific antigen (PSA) sensing, which demonstrates the biocompatibility and applied potency of this proposed self-contained system in point-of-care biomedical applications.

On the other hand, the zero-order symmetrical Lamb wave mode, S_0, becomes a longitudinal wave when the layer thickness approaches zero. At higher frequencies, the extensional mode converges toward the Rayleigh mode. Membrane-based thin film Lamb wave devices have been used for biosensing, especially for applications in a liquid environment.[146] Compared with the A_0 mode, the S_0 mode is more preferred for liquid sensing because of its higher phase velocities and low phase velocity dispersion. The $Si/SiO_2/Si_3N_4$/Cr/Au/ZnO Lamb wave device was used to detect the concentration of immunoglobulin E (IgE) in human serum, with a sensitivity as high as 8.52×10^7 cm^2 g^{-1} at a wave frequency of 9 MHz.[147] Another flexible AlN-based lamb wave immunosensor fabricated on recyclable polyethylene naphthalate substrate was applied to detect *E. coli*, showing a better sensitivity compared with sensor fabricated on silicon substrate, with a limit of detection of 6.54×10^5 CFU mL^{-1} (ref. 148) (Fig. 14c).

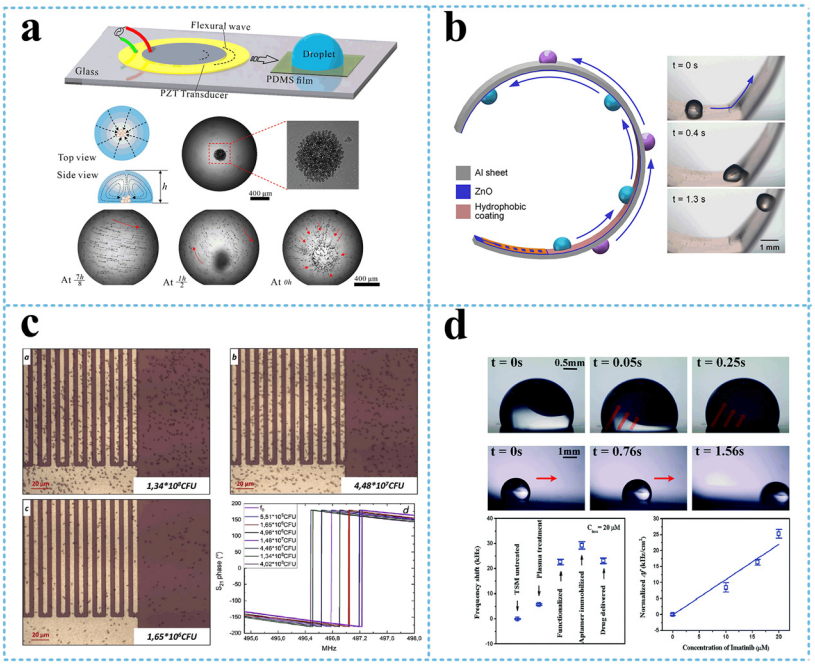

Fig. 14 Flexible SAW devices based on the Lamb wave. a: Schematic and experimental presentation of the lamb wave-based concentration device;[143] b: schematic and experimental presentation of droplet transportation along a curved surface using a flexible SAW device (reproduced from ref. 144 with permission from American Chemical Society, copyright 2021); c: optical micrograph and S_{21} phase change of bacterial adhesion at increasing concentration on a Lamb wave-based biosensor (reproduced from ref. 148 with permission from Elsevier, copyright 2020); d: experimental presentation of a flexible acoustic device integrating microfluids and biosensing (Reproduced from ref. 140 with permission from the Royal Society of Chemistry, copyright 2020).

In addition to the A_0 and S_0 mode Lamb waves generated from the IDTs, a lateral field excitation of thickness shear mode (LFE-TSM) wave (a typical shear bulk acoustic wave) can also be generated using two electrodes deposited on top of a piezoelectric substrate or thin film. Higher order modes of the Lamb waves rather than the S_0 modes can achieve better sensitivity for applications due to their high phase velocity, low phase velocity dispersion, and lower impedance.[149] Tao *et al.*[140] reported a flexible ZnO/Al acoustic device that can excite both the lamb wave mode and LFE-TSM mode individually at their resonant frequencies, enabling to perform sampling, patterning, and biosensing selectively in a single device. Lamb waves were excited for sample dilution and transport by adjusting the input SAW power, while the LFE-TSM waves enabled particles patterning by agitating fundamental orders with low input power as well as biosensing by monitoring the frequency shifts for higher order waves (Fig. 14d).

7. Conclusion and outlook

After the development of half a century, SAW devices have been widely used in various fields, especially in the field of biological detection. We presented theoretical and experimental evidence of the advantage of using SAWs as sensors and actuators. In short, the roles of SAWs in biological detection can be summarized as two aspects: (1) as actuators for sample pretreatment process, including the sorting, enrichment, mixing of biological particles, and the heating of liquid samples; (2) as biosensors for the qualitative or quantitative detection of various biological objectives. To accomplish such functions, four types of SAWs are included and discussed in this work.

Rayleigh SAW separation techniques have various advantages including favorable biocompatibility, non-invasive features, and relatively high sorting efficiency. These techniques allow sorting and purifying micron-sized cells and submicron bioparticles within the microfluidics chip, and it has become a very promising alternative used for sample pretreatment in research and clinical applications. However, the relatively low throughput of current acoustofluidic devices is inadequate for the rapid processing of large amounts of samples for clinical applications. Because excessive throughput sometimes leads to a decrease in separation efficiency, it is a great challenge to strike a balance between sorting performance and throughput. Benefiting from the high integration capacity of microfluidic chips, it is possible to introduce the concept of "parallel treatment" into the fields and make the multiple chips procced along the biological samples simultaneously to satisfy the demand of large throughput in practical situations.

Meanwhile, for SAW biosensors, SH-SAW devices with a guiding layer or LW-SAW devices between the IDTs region are

the most used platform for biosensing applications in liquids due to their waveguiding layer that can confine acoustic waves energy at the piezoelectric surface and high sensitivity to surface modification. Although they have several advantages over traditional bioassays in their fast responsiveness, small size, and high sensitivity, but they still suffer many challenges such as controlling the film thickness, the damping effect in liquid detection, the incompatibility of some piezoelectric substrates with complementary metal oxide semiconductor, high cost of packaging, and difficulties in integrating microfluids. Nouveau materials and fabrication should be developed to solve the above problems.

Recently, membrane-based flexible lamb wave devices have been developed for microfluidic actuation of liquids and biosensing. The A_0 mode lamb wave devices can radiate wave energy into the surrounding medium, causing acoustic streaming parallel to the device surface, and have been proposed for mixing and pumping applications. While the S_0 mode lamb wave devices are more preferred for liquid sensing because of its higher phase velocities and low phase velocity dispersion, the use of piezoelectric thin film material permits the deposition and localization of the film solely on the SAW propagation region through micromachining and also makes it possible to incorporate various functions such as wearability and tactility. Furthermore, flexible polymeric SAW biosensors have gained more attention because of their relatively low-cost, recyclability, and the ability to monitor changes wirelessly. Fabricating SAW devices on inexpensive and flexible substrates has a huge potential for the production of wearable, disposable, or recyclable applications.

The real-time, label-free sensing capability of acoustic biosensors and microfluidic actuation platforms with sensitive performance relevant to the clinical levels makes them a suitable candidate for integrated devices, enabling quick disease diagnosis in the area of medical research. The advantage of less sample preparation and faster sensing capabilities and the simplicity in the usage of piezoelectric biosensors and microfluidic platforms enable SAW devices to be a promising candidate for lab-on-chip applications in several fields, such as clinical diagnosis, laboratory research, food safety, and environmental monitoring.

Author contributions

The manuscript was written through contributions of all authors.

Conflicts of interest

The authors declare that they have no known competing financial interests or personal relationships that could have appeared to influence the work reported in this paper.

Acknowledgements

This work is financially supported by the National Key R&D Program of China (2022YFC2406600) and Program for Innovation Team of Shaanxi Province (2021TD-23).

References

1 G. M. Whitesides, The origins and the future of microfluidics, *Nature*, 2006, **442**, 368–373.
2 X. Qin, X. Wei, L. Li, H. Wang, Z. Jiang and D. Sun, Acoustic valves in microfluidic channels for droplet manipulation, *Lab Chip*, 2021, **21**, 3165–3173.
3 C. Zhang, P. Brunet, L. Royon and X. Guo, Mixing intensification using sound-driven micromixer with sharp edges, *Chem. Eng. J.*, 2020, **410**, 128252.
4 P. Teng, D. Tian, H. Fu and S. Wang, Recent progress of electrowetting for droplet manipulation: from wetting to superwetting systems, *Mater. Chem. Front.*, 2020, **4**, 140–154.
5 G. Chen, B. Ji, Y. Gao, C. Wang, J. Wu, B. Zhou and W. Wen, Towards the rapid and efficient mixing on 'open-surface' droplet-based microfluidics via magnetic actuation, *Sens. Actuators, B*, 2019, **286**, 181–190.
6 H. Yang and M. A. Gijs, Micro-optics for microfluidic analytical applications, *Chem. Soc. Rev.*, 2018, **47**, 1391–1458.
7 L. Rayleigh, On waves propagated along the plane surface of an elastic solid, *Proc. London Math. Soc.*, 1885, **1**, 4–11.
8 R. M. White and F. W. Voltmer, Direct piezoelectric coupling to surface elastic waves, *Appl. Phys. Lett.*, 1965, **7**, 314–316.
9 Y. Liu, Y. Cai, Y. Zhang, A. Tovstopyat, S. Liu and C. Sun, Materials, Design, and Characteristics of Bulk Acoustic Wave Resonator: A Review, *Micromachines*, 2020, **11**, 630.
10 A. Lenshof, M. Evander, T. Laurell and J. Nilsson, Acoustofluidics 5: Building microfluidic acoustic resonators, *Lab Chip*, 2012, **12**, 684–695.
11 K. Länge, Bulk and Surface Acoustic Wave Sensor Arrays for Multi-Analyte Detection: A Review, *Sensors*, 2019, **19**, 5382.
12 P. Delsing, A. N. Cleland, M. J. Schuetz, J. Knörzer, G. Giedke, J. I. Cirac, K. Srinivasan, M. Wu, K. C. Balram and C. Bäuerle, The 2019 surface acoustic waves roadmap, *J. Phys. D: Appl. Phys.*, 2019, **52**, 353001.
13 B. Liu, X. Chen, H. Cai, M. M. Ali, X. Tian, L. Tao, Y. Yang and T. Ren, Surface acoustic wave devices for sensor applications, *J. Semicond.*, 2016, **37**, 021001.
14 C. Campbell, *Surface Acoustic Wave Devices for Mobile and Wireless Communications, Four-Volume Set*, Academic press, 1998.
15 L. Shao, D. Zhu, M. Colangelo, D. Lee, N. Sinclair, Y. Hu, P. T. Rakich, K. Lai, K. K. Berggren and M. Lončar, Electrical control of surface acoustic waves, *Nat. Electron.*, 2022, 1–8.
16 Y. Yoshino, T. Makino, Y. Katayama and T. Hata, Optimization of zinc oxide thin film for surface acoustic

wave filters by radio frequency sputtering, *Vacuum*, 2000, **59**, 538–545.
17 C. C. Ruppel, Acoustic wave filter technology–a review, *IEEE Trans. Ultrason. Ferroelectr. Freq. Control*, 2017, **64**, 1390–1400.
18 V. Peri, Z.-D. Song, M. Serra-Garcia, P. Engeler, R. Queiroz, X. Huang, W. Deng, Z. Liu, B. A. Bernevig and S. D. Huber, Experimental characterization of fragile topology in an acoustic metamaterial, *Science*, 2020, **367**, 797–800.
19 A. Okada, F. Oguro, A. Noguchi, Y. Tabuchi, R. Yamazaki, K. Usami and Y. Nakamura, Cavity enhancement of anti-stokes scattering via optomechanical coupling with surface acoustic waves, *Phys. Rev. Appl.*, 2018, **10**, 024002.
20 J. R. Lane, Integrating Superconducting Qubits with Quantum Fluids and Surface Acoustic Wave Devices, *PhD thesis*, Michigan State University, 2021.
21 G. Andersson, M. K. Ekström and P. Delsing, Electromagnetically induced acoustic transparency with a superconducting circuit, *Phys. Rev. Lett.*, 2020, **124**, 240402.
22 D. Li, X. Zu, D. Ao, Q. Tang, Y. Fu, Y. Guo, K. Bilawal, M. B. Faheem, L. Li and S. Li, High humidity enhanced surface acoustic wave (SAW) H2S sensors based on sol–gel CuO films, *Sens. Actuators, B*, 2019, **294**, 55–61.
23 X. Zhou, Q. Tan, X. Liang, B. Lin, T. Guo and Y. Gan, Novel multilayer SAW temperature sensor for ultra-high temperature environments, *Micromachines*, 2021, **12**, 643.
24 J. Ji, C. Yang, F. Zhang, Z. Shang, Y. Xu, Y. Chen, M. Chen and X. Mu, A high sensitive SH-SAW biosensor based 36 YX black $LiTaO_3$ for label-free detection of Pseudomonas Aeruginosa, *Sens. Actuators, B*, 2019, **281**, 757–764.
25 H.-Y. Li, W.-N. Jia, X.-Y. Li, L. Zhang, C. Liu and J. Wu, Advances in detection of infectious agents by aptamer-based technologies, *Emerging Microbes Infect.*, 2020, **9**, 1671–1681.
26 L. Lamanna, F. Rizzi, V. R. Bhethanabotla and M. De Vittorio, Conformable surface acoustic wave biosensor for E-coli fabricated on PEN plastic film, *Biosens. Bioelectron.*, 2020, **163**, 112164.
27 P. Jahanshahi, Q. Wei, Z. Jie and E. Zalnezhad, Designing a non-invasive surface acoustic resonator for ultra-high sensitive ethanol detection for an on-the-spot health monitoring system, *Biotechnol. Bioprocess Eng.*, 2018, **23**, 394–404.
28 Y. Li, J. Li, J. Huang and H. Zhou, Fitting analysis and research of measured data of SAW micro-pressure sensor based on BP neural network, *Measurement*, 2020, **155**, 107533.
29 H. Hallil, Q. Zhang, E. Flahaut, J.-L. Lachaud, P. Coquet, C. Dejous and D. Rebière, Guided SH-SAW sensor based on DWNTs sensitive material for VOCs and humidity detection, *J. Integr. Circuits Syst.*, 2018, **13**, 1–4.
30 Z. Li, Guided shear-horizontal surface acoustic wave (SH-SAW) chemical sensors for detection of organic contaminants in aqueous environments, *PhD thesis*, Marquette University, 2005.
31 S. Liu, H. Sun, R. Nagarajan, J. Kumar, Z. Gu, J. Cho and P. Kurup, Dynamic chemical vapor sensing with nanofibrous film based surface acoustic wave sensors, *Sens. Actuators, A*, 2011, **167**, 8–13.
32 D. L. Arruda, W. C. Wilson, C. Nguyen, Q. W. Yao, R. J. Caiazzo, I. Talpasanu, D. E. Dow and B. C. Liu, Microelectrical sensors as emerging platforms for protein biomarker detection in point-of-care diagnostics, *Expert Rev. Mol. Diagn.*, 2009, **9**, 749–755.
33 D. Morgan, *Surface acoustic wave filters: With applications to electronic communications and signal processing*, Academic Press, 2010.
34 D. L. Miller, N. B. Smith, M. R. Bailey, G. J. Czarnota, K. Hynynen, I. R. S. Makin and Bioeffects Committee of the American Institute of Ultrasound in Medicine, Overview of therapeutic ultrasound applications and safety considerations, *J. Ultrasound Med.*, 2012, **31**, 623–634.
35 X. Ding, P. Li, S.-C. S. Lin, Z. S. Stratton, N. Nama, F. Guo, D. Slotcavage, X. Mao, J. Shi and F. Costanzo, Surface acoustic wave microfluidics, *Lab Chip*, 2013, **13**, 3626–3649.
36 Y. Fan, X. Wang, J. Ren, F. Lin and J. Wu, Recent advances in acoustofluidic separation technology in biology, *Microsyst. Nanoeng.*, 2022, **8**, 1–16.
37 E. El Boudouti, B. Djafari-Rouhani, A. Akjouj and L. Dobrzynski, Acoustic waves in solid and fluid layered materials, *Surf. Sci. Rep.*, 2009, **64**, 471–594.
38 J. Cheeke, *Fundamentals and Applications of Ultrasonic Waves*, CRC press, 2010.
39 H. Mitome, The mechanism of generation of acoustic streaming, *Electron. Commun. Jpn.*, 1998, **81**, 1–8.
40 N. Riley, Steady streaming, *Annu. Rev. Fluid Mech.*, 2001, **33**, 43.
41 R. B. Bird, Transport phenomena, *Appl. Mech. Rev.*, 2002, **55**(1), R1–R4.
42 J. Dual, P. Hahn, I. Leibacher, D. Möller, T. Schwarz and J. Wang, Acoustofluidics 19: Ultrasonic microrobotics in cavities: devices and numerical simulation, *Lab Chip*, 2012, **12**, 4010–4021.
43 H. Bruus, Acoustofluidics 7: The acoustic radiation force on small particles, *Lab Chip*, 2012, **12**, 1014–1021.
44 J. Dual, P. Hahn, I. Leibacher, D. Moller, T. Schwarz and J. Wang, Acoustofluidics 19: ultrasonic microrobotics in cavities: devices and numerical simulation, *Lab Chip*, 2012, **12**, 4010–4021.
45 D. Mandal and S. Banerjee, Surface Acoustic Wave (SAW) Sensors: Physics, Materials, and Applications, *Sensors*, 2022, **22**, 820.
46 Y. Chen, S. Li, Y. Gu, P. Li, X. Ding, L. Wang, J. P. McCoy, S. J. Levine and T. J. Huang, Continuous enrichment of low-abundance cell samples using standing surface acoustic waves (SSAW), *Lab Chip*, 2014, **14**, 924–930.
47 M. Agostini, F. Lunardelli, M. Gagliardi, A. Miranda, L. Lamanna, A. G. Luminare, F. Gambineri, M. Lai, M. Pistello and M. Cecchini, Surface-Acoustic-Wave (SAW) Induced Mixing Enhances the Detection of Viruses: Application to

Measles Sensing in Whole Human Saliva with a SAW Lab-On-a-Chip, *Adv. Funct. Mater.*, 2022, **32**(44), 2201958.

48 T. Roux-Marchand, D. Beyssen, F. Sarry and O. Elmazria, Rayleigh surface acoustic wave as an efficient heating system for biological reactions: investigation of microdroplet temperature uniformity, *IEEE Trans. Ultrason. Ferroelectr. Freq. Control*, 2015, **62**, 729–735.

49 Y. Gao, M. Wu, Y. Lin and J. Xu, Acoustic Microfluidic Separation Techniques and Bioapplications: A Review, *Micromachines*, 2020, **11**(10), 921.

50 Y. Fan, X. Wang, J. Ren, F. Lin and J. Wu, Recent advances in acoustofluidic separation technology in biology, *Microsyst. Nanoeng.*, 2022, **8**, 94.

51 X. Lu, A. Martin, F. Soto, P. Angsantikul, J. Li, C. Chen, Y. Liang, J. Hu, L. Zhang and J. Wang, Parallel Label-Free Isolation of Cancer Cells Using Arrays of Acoustic Microstreaming Traps, *Adv. Mater. Technol.*, 2018, **4**(2), 1800374.

52 H. Liu, Z. Ao, B. Cai, X. Shu, K. Chen, L. Rao, C. Luo, F.-B. Wang, W. Liu, M. Bondesson, S. Guo and F. Guo, Size-amplified acoustofluidic separation of circulating tumor cells with removable microbeads, *Nano Futures*, 2018, **2**, 025004.

53 Z. Ma, Y. Zhou, D. J. Collins and Y. Ai, Fluorescence activated cell sorting via a focused traveling surface acoustic beam, *Lab Chip*, 2017, **17**, 3176–3185.

54 Y. Zhou, Z. Ma and Y. Ai, Hybrid microfluidic sorting of rare cells based on high throughput inertial focusing and high accuracy acoustic manipulation, *RSC Adv.*, 2019, **9**, 31186–31195.

55 K. Mutafopulos, P. Spink, C. D. Lofstrom, P. J. Lu, H. Lu, J. C. Sharpe, T. Franke and D. A. Weitz, Traveling surface acoustic wave (TSAW) microfluidic fluorescence activated cell sorter (muFACS), *Lab Chip*, 2019, **19**, 2435–2443.

56 W. L. Ung, K. Mutafopulos, P. Spink, R. W. Rambach, T. Franke and D. A. Weitz, Enhanced surface acoustic wave cell sorting by 3D microfluidic-chip design, *Lab Chip*, 2017, **17**, 4059–4069.

57 Z. Liu, Y. Lei, Z. Yu, Z. Meng, S. Jin, X. Qu, Z. Jiang, F. Zhang and X. Wei, Fluorescent labeling based acoustofluidic screening of Japanese encephalitis virus, *Sens. Actuators, B*, 2020, **322**, 128649.

58 R. Ahmad, G. Destgeer, M. Afzal, J. Park, H. Ahmed, J. H. Jung, K. Park, T. S. Yoon and H. J. Sung, Acoustic Wave-Driven Functionalized Particles for Aptamer-Based Target Biomolecule Separation, *Anal. Chem.*, 2017, **89**, 13313–13319.

59 J. P. Muhammad Afzal, Ghulam Destgeer, Husnain Ahmed, Syed Atif Iqrar, Sanghee Kim, Sunghyun Kang, Anas Alazzam, Tae-Sung Yoon, Hyung Jin Sung, Acoustomicrofluidic separation of tardigrades from raw cultures for sample preparation, *Zoological Journal of the Linnean Society*, 2020, **188**, 809–819.

60 M. Afzal, J. Park, J. S. Jeon, M. Akmal, T. S. Yoon and H. J. Sung, Acoustofluidic Separation of Proteins Using Aptamer-Functionalized Microparticles, *Anal. Chem.*, 2021, **93**, 8309–8317.

61 X. Ding, S. C. Lin, M. I. Lapsley, S. Li, X. Guo, C. Y. Chan, I. K. Chiang, L. Wang, J. P. McCoy and T. J. Huang, Standing surface acoustic wave (SSAW) based multichannel cell sorting, *Lab Chip*, 2012, **12**, 4228–4231.

62 J. Nam, H. Lim, D. Kim and S. Shin, Separation of platelets from whole blood using standing surface acoustic waves in a microchannel, *Lab Chip*, 2011, **11**, 3361–3364.

63 B. L. Gray, H. Becker, Y. Ai and B. L. Marrone, presented in part at the *Microfluidics, BioMEMS, and Medical Microsystems XII*, 2014.

64 G. Simon, C. Busch, M. A. B. Andrade, J. Reboud, J. M. Cooper, M. P. Y. Desmulliez, M. O. Riehle and A. L. Bernassau, Bandpass sorting of heterogeneous cells using a single surface acoustic wave transducer pair, *Biomicrofluidics*, 2021, **15**, 014105.

65 X. Ding, Z. Peng, S. C. Lin, M. Geri, S. Li, P. Li, Y. Chen, M. Dao, S. Suresh and T. J. Huang, Cell separation using tilted-angle standing surface acoustic waves, *Proc. Natl. Acad. Sci. U. S. A.*, 2014, **111**, 12992–12997.

66 P. Li, Z. Mao, Z. Peng, L. Zhou, Y. Chen, P. H. Huang, C. I. Truica, J. J. Drabick, W. S. El-Deiry, M. Dao, S. Suresh and T. J. Huang, Acoustic separation of circulating tumor cells, *Proc. Natl. Acad. Sci. U. S. A.*, 2015, **112**, 4970–4975.

67 M. Wu, K. Chen, S. Yang, Z. Wang, P. H. Huang, J. Mai, Z. Y. Li and T. J. Huang, High-throughput cell focusing and separation via acoustofluidic tweezers, *Lab Chip*, 2018, **18**, 3003–3010.

68 Y. Xie, Z. Mao, H. Bachman, P. Li, P. Zhang, L. Ren, M. Wu and T. J. Huang, Acoustic Cell Separation Based on Density and Mechanical Properties, *J. Biomech. Eng.*, 2020, **142**(3), 0310051–0310059.

69 L. Meng, X. Cui, C. Dong, X. Liu, W. Zhou, W. Zhang, X. Wang, L. Niu, F. Li, F. Cai, J. Wu and H. Zheng, Microbubble enhanced acoustic tweezers for size-independent cell sorting, *Appl. Phys. Lett.*, 2020, **116**, 073701.

70 X. J. Hu, H. L. Liu, Y. X. Jin, L. Liang, D. M. Zhu, X. Q. Zhu, S. S. Guo, F. L. Zhou and Y. Yang, Precise label-free leukocyte subpopulation separation using hybrid acoustic-optical chip, *Lab Chip*, 2018, **18**, 3405–3412.

71 A. A. Nawaz, M. Urbanska, M. Herbig, M. Notzel, M. Krater, P. Rosendahl, C. Herold, N. Toepfner, M. Kubankova, R. Goswami, S. Abuhattum, F. Reichel, P. Muller, A. Taubenberger, S. Girardo, A. Jacobi and J. Guck, Intelligent image-based deformation-assisted cell sorting with molecular specificity, *Nat. Methods*, 2020, **17**, 595–599.

72 Z. Pei, Y. Ma, C. Wang, Y. Wu, F. Song and X. Wu, Optimal design of a driver of interdigital transducers used to generate standing surface acoustic waves for cell sorting, *Rev. Sci. Instrum.*, 2021, **92**, 034705.

73 Y. Ai, C. K. Sanders and B. L. Marrone, Separation of Escherichia coli bacteria from peripheral blood mononuclear cells using standing surface acoustic waves, *Anal. Chem.*, 2013, **85**, 9126–9134.

74 S. Li, F. Ma, H. Bachman, C. E. Cameron, X. Zeng and T. J. Huang, Acoustofluidic bacteria separation, *J. Micromech. Microeng.*, 2017, **27**(1), 015031.

75 S. Ning, S. Liu, Y. Xiao, G. Zhang, W. Cui and M. Reed, A microfluidic chip with a serpentine channel enabling high-throughput cell separation using surface acoustic waves, *Lab Chip*, 2021, **21**, 4608–4617.
76 H. S. Kyungheon Lee, R. Weissleder and H. Lee, Acoustic Purification of Extracellular Microvesicles, *ACS Nano*, 2015, **9**, 2321–2327.
77 M. Tayebi, D. Yang, D. J. Collins and Y. Ai, Deterministic Sorting of Submicrometer Particles and Extracellular Vesicles Using a Combined Electric and Acoustic Field, *Nano Lett.*, 2021, **21**, 6835–6842.
78 M. Wu, Y. Ouyang, Z. Wang, R. Zhang, P. H. Huang, C. Chen, H. Li, P. Li, D. Quinn, M. Dao, S. Suresh, Y. Sadovsky and T. J. Huang, Isolation of exosomes from whole blood by integrating acoustics and microfluidics, *Proc. Natl. Acad. Sci. U. S. A.*, 2017, **114**, 10584–10589.
79 Z. Y. Wang, F. Li, J. Rufo, C. Y. Chen, S. J. Yang, L. Li, J. X. Zhang, J. Cheng, Y. Kim, M. X. Wu, E. Abemayor, M. Tu, D. Chia, R. Spruce, N. Batis, H. Mehanna, D. T. W. Wong and T. J. Huang, Acoustofluidic Salivary Exosome Isolation A Liquid Biopsy Compatible Approach for Human Papillomavirus-Associated Oropharyngeal Cancer Detection, *J. Mol. Diagn.*, 2020, **22**, 50–59.
80 Z. Wang, H. Wang, R. Becker, J. Rufo, S. Yang, B. E. Mace, M. Wu, J. Zou, D. T. Laskowitz and T. J. Huang, Acoustofluidic separation enables early diagnosis of traumatic brain injury based on circulating exosomes, *Microsyst. Nanoeng.*, 2021, **7**, 20.
81 N. Hao, Z. Wang, P. Liu, R. Becker, S. Yang, K. Yang, Z. Pei, P. Zhang, J. Xia, L. Shen, L. Wang, K. A. Welsh-Bohmer, L. Sanders, L. P. Lee and T. J. Huang, Acoustofluidic multimodal diagnostic system for Alzheimer's disease, *Biosens. Bioelectron.*, 2022, **196**, 113730.
82 G. S. Calabrese, H. Wohltjen and M. K. Roy, Surface acoustic wave devices as chemical sensors in liquids. Evidence disputing the importance of Rayleigh wave propagation, *Anal. Chem.*, 1987, **59**, 833–837.
83 J. Kondoh, Y. Matsui, S. Shiokawa and W. B. Wlodarski, Enzyme-immobilized SH-SAW biosensor, *Sens. Actuators, B*, 1994, **20**, 199–203.
84 X. C. Lo, J. Y. Li, M. T. Lee and D. J. Yao, Frequency Shift of a SH-SAW Biosensor with Glutaraldehyde and 3-Aminopropyltriethoxysilane Functionalized Films for Detection of Epidermal Growth Factor, *Biosensors*, 2020, **10**(8), 92.
85 K. Lange, B. E. Rapp and M. Rapp, Surface acoustic wave biosensors: a review, *Anal. Bioanal. Chem.*, 2008, **391**, 1509–1519.
86 J. Ji, Y. Pang, D. Li, Z. Huang, Z. Zhang, N. Xue, Y. Xu and X. Mu, An aptamer-based shear horizontal surface acoustic wave biosensor with a CVD-grown single-layered graphene film for high-sensitivity detection of a label-free endotoxin, *Microsyst. Nanoeng.*, 2020, **6**, 4.
87 F. Josse, F. Bender and R. W. Cernosek, Guided Shear Horizontal Surface Acoustic Wave Sensors for Chemical and Biochemical Detection in Liquids, *Anal. Chem.*, 2001, **73**, 5937–5944.
88 O. Onen, A. Sisman, N. D. Gallant, P. Kruk and R. Guldiken, A Urinary Bcl-2 Surface Acoustic Wave Biosensor for Early Ovarian Cancer Detection, *Sensors*, 2012, **12**, 7423–7437.
89 A. Pomowski, C. Baricham, B. E. Rapp, A. Matern and K. Lange, Acoustic Biosensors Coated With Phosphorylcholine Groups for Label-Free Detection of Human C-Reactive Protein in Serum, *IEEE Sens. J.*, 2015, **15**, 4388–4392.
90 Y. C. Peng, C. H. Cheng, H. Yatsuda, S. H. Liu, S. J. Liu, T. Kogai, C. Y. Kuo and R. Y. L. Wang, A Novel Rapid Test to Detect Anti-SARS-CoV-2 N Protein IgG Based on Shear Horizontal Surface Acoustic Wave (SH-SAW), *Diagnostics*, 2021, **11**(10), 1838.
91 S. Trivedi and H. B. Nemade, Highly Sensitive SH-SAW Resonator with SiO2 trenches for Biosensing Application, *Mater. Today: Proc.*, 2017, **4**, 10427–10431.
92 N. Fourati, M. Lazerges, C. Védrine, J.-M. Fougnion, C. Zerrouki, L. Rousseau, P. Lepeut, J. J. Bonnet and C. Pernelle, Surface Acoustic Waves Sensor for DNA-Biosensor Development, *Sens. Lett.*, 2009, **7**, 847–850.
93 D. Matatagui, A. Bastida and M. C. Horrillo, Novel SH-SAW Biosensors for Ultra-Fast Recognition of Growth Factors, *Biosensors*, 2021, **12**(1), 17.
94 F. Di Pietrantonio, M. Benetti, D. Cannatà, E. Verona, M. Girasole, M. Fosca, S. Dinarelli, M. Staiano, V. M. Marzullo, A. Capo, A. Varriale and S. D'Auria, A Shear horizontal surface acoustic wave biosensor for a rapid and specific detection of d-serine, *Sens. Actuators, B*, 2016, **226**, 1–6.
95 M. S. Brugger, L. G. Schnitzler, T. Nieberle, A. Wixforth and C. Westerhausen, Shear-horizontal surface acoustic wave sensor for non-invasive monitoring of dynamic cell spreading and attachment in wound healing assays, *Biosens. Bioelectron.*, 2021, **173**, 112807.
96 T. Higashiyama, A. Katsuyama, H. Otori, T. Kamimura, A. Uehara, M. Kainuma, R. Takumi, Y. Kudo, M. Ebina, K. Mochitate, T. Kon, Y. Furuya and H. Kikuchi, Detection of cellular damage by hydrogen peroxide using SV40-T2 cells on shear horizontal surface acoustic wave (SH-SAW) sensor, *Ultrasonics*, 2014, **54**, 1430–1438.
97 J. T. Baca, V. Severns, D. Lovato, D. W. Branch and R. S. Larson, Rapid detection of Ebola virus with a reagent-free, point-of-care biosensor, *Sensors*, 2015, **15**, 8605–8614.
98 E. R. Gray, V. Turbe, V. E. Lawson, R. H. Page, Z. C. Cook, R. B. Ferns, E. Nastouli, D. Pillay, H. Yatsuda, D. Athey and R. A. McKendry, Ultra-rapid, sensitive and specific digital diagnosis of HIV with a dual-channel SAW biosensor in a pilot clinical study, *NPJ Digit. Med.*, 2018, **1**, 35.
99 E. Berkenpas, P. Millard and M. Pereira da Cunha, Detection of Escherichia coli O157:H7 with langasite pure shear horizontal surface acoustic wave sensors, *Biosens. Bioelectron.*, 2006, **21**, 2255–2262.
100 S. T. Ten, U. Hashim, S. C. B. Gopinath, W. W. Liu, K. L. Foo, S. T. Sam, S. F. A. Rahman, C. H. Voon and A. N. Nordin, Highly sensitive Escherichia coli shear horizontal surface acoustic wave biosensor with silicon dioxide nanostructures, *Biosens. Bioelectron.*, 2017, **93**, 146–154.

101 M. I. Gaso Rocha, Y. Jimenez, F. A. Laurent and A. Arnau, in *State of the Art in Biosensors - General Aspects*, 2013, ch. 11, DOI: **10.5772/53077**.
102 Y. Huang, P. K. Das and V. R. Bhethanabotla, Surface acoustic waves in biosensing applications, *Sensors and Actuators Reports*, 2021, **3**, 100041.
103 S. I. Zida, Y. D. Lin and Y. L. Khung, Current Trends on Surface Acoustic Wave Biosensors, *Adv. Mater. Technol.*, 2021, **6**(6), 2001018.
104 B. Liu, X. Chen, H. Cai, M. Mohammad Ali, X. Tian, L. Tao, Y. Yang and T. Ren, Surface acoustic wave devices for sensor applications, *J. Semicond.*, 2016, **37**, 021001.
105 Z. Xu and Y. J. Yuan, Implementation of guiding layers of surface acoustic wave devices: A review, *Biosens. Bioelectron.*, 2018, **99**, 500–512.
106 D. Mandal and S. Banerjee, Surface Acoustic Wave (SAW) Sensors: Physics, Materials, and Applications, *Sensors*, 2022, **22**(3), 820.
107 M. Agostini and M. Cecchini, Ultra-high-frequency (UHF) surface-acoustic-wave (SAW) microfluidics and biosensors, *Nanotechnology*, 2021, **32**(31), 312001.
108 S. Krishnamoorthy, A. A. Iliadis, T. Bei and G. P. Chrousos, An interleukin-6 $ZnO/SiO_2/Si$ surface acoustic wave biosensor, *Biosens. Bioelectron.*, 2008, **24**, 313–318.
109 H. Oh, W. Wang, K. Lee, H. C. Yoon and S. Yang, Wirelessly Driven and Battery-Free Love Wave Biosensor Based on Dinitrophenyl Immobilization, *Jpn. J. Appl. Phys.*, 2009, **48**, 06FJ05.
110 Y. Zou, X. Zhang, C. An, C. Ran, K. Ying and P. Wang, A point-of-care testing system with Love-wave sensor and immunogold staining enhancement for early detection of lung cancer, *Biomed. Microdevices*, 2014, **16**, 927–935.
111 Y. Zhang, F. Yang, Z. Sun, Y.-T. Li and G.-J. Zhang, A surface acoustic wave biosensor synergizing DNA-mediated in situ silver nanoparticle growth for a highly specific and signal-amplified nucleic acid assay, *Analyst*, 2017, **142**, 3468–3476.
112 J. Ji, Y. Pang, D. Li, X. Wang, Y. Xu and X. Mu, Single-Layered Graphene/Au-Nanoparticles-Based Love Wave Biosensor for Highly Sensitive and Specific Detection of Staphylococcus aureus Gene Sequences, *ACS Appl. Mater. Interfaces*, 2020, **12**, 12417–12425.
113 J. Luo, M. Xie, P. Luo, B. Zhao, K. Du and P. Fan, A sensitive glucose biosensor without using glucose test strips based on $ZnO/SiO_2/Si$ surface acoustic wave device, *Mater. Lett.*, 2014, **130**, 14–16.
114 L. Rana, R. Gupta, M. Tomar and V. Gupta, Highly sensitive Love wave acoustic biosensor for uric acid, *Sens. Actuators, B*, 2018, **261**, 169–177.
115 J. Han, M. Li, H. Li, H. Li, C. Li, H. Li, L. Qian and B. Yang, A 433-MHz surface acoustic wave sensor with Ni-TiO2-poly(L-lysine) composite film for dopamine determination, *Microchim. Acta*, 2020, **187**(12), 671.
116 M. Saitakis, A. Tsortos and E. Gizeli, Probing the interaction of a membrane receptor with a surface-attached ligand using whole cells on acoustic biosensors, *Biosens. Bioelectron.*, 2010, **25**, 1688–1693.
117 P. Bröker, K. Lücke, M. Perpeet and T. M. A. Gronewold, A nanostructured SAW chip-based biosensor detecting cancer cells, *Sens. Actuators, B*, 2012, **165**, 1–6.
118 H. Wu, H. Zu, J. H. C. Wang and Q.-M. Wang, A study of Love wave acoustic biosensors monitoring the adhesion process of tendon stem cells (TSCs), *Eur. Biophys. J.*, 2019, **48**, 249–260.
119 Y. Jiang, C. Y. Tan, S. Y. Tan, M. S. F. Wong, Y. F. Chen, L. Zhang, K. Yao, S. K. E. Gan, C. Verma and Y.-J. Tan, SAW sensor for Influenza A virus detection enabled with efficient surface functionalization, *Sens. Actuators, B*, 2015, **209**, 78–84.
120 Z. Xu and Y. J. Yuan, Quantification of Staphylococcus aureususing surface acoustic wave sensors, *RSC Adv.*, 2019, **9**, 8411–8414.
121 H. J. Lee, K. Namkoong, E. C. Cho, C. Ko, J. C. Park and S. S. Lee, Surface acoustic wave immunosensor for real-time detection of hepatitis B surface antibodies in whole blood samples, *Biosens. Bioelectron.*, 2009, **24**, 3120–3125.
122 E. Gizeli, N. J. Goddard, C. R. Lowe and A. C. Stevenson, A love plate biosensor utilising a polymer layer Sensors, *Sens. Actuators, B*, 1992, **6**, 131–137.
123 J. Freudenberg, S. Schelle, K. Beck, M. V. Schickfus and S. Hunklinger, A contactless surface acoustic wave biosensor, *Biosens. Bioelectron.*, 1999, **14**(4), 423–425.
124 S. Lee, K.-B. Kim and Y.-I. Kim, Love wave SAW biosensors for detection of antigen-antibody binding and comparison with SPR biosensor, *Food Sci. Biotechnol.*, 2011, **20**, 1413–1418.
125 A. Tretjakov, V. Syritski, J. Reut, R. Boroznjak and A. Öpik, Molecularly imprinted polymer film interfaced with Surface Acoustic Wave technology as a sensing platform for label-free protein detection, *Anal. Chim. Acta*, 2016, **902**, 182–188.
126 X. Zhang, Y. Zou, C. An, K. Ying, X. Chen and P. Wang, Sensitive detection of carcinoembryonic antigen in exhaled breath condensate using surface acoustic wave immunosensor, *Sens. Actuators, B*, 2015, **217**, 100–106.
127 S. Li, Y. Wan, Y. Su, C. Fan and V. R. Bhethanabotla, Gold nanoparticle-based low limit of detection Love wave biosensor for carcinoembryonic antigens, *Biosens. Bioelectron.*, 2017, **95**, 48–54.
128 P. J. Jandas, J. Luo, A. Quan, C. Qiu, W. Cao, C. Fu and Y. Q. Fu, Highly selective and label-free Love-mode surface acoustic wave biosensor for carcinoembryonic antigen detection using a self-assembled monolayer bioreceptor, *Appl. Surf. Sci.*, 2020, **518**(15), 146061.
129 P. J. Jandas, J. Luo, K. Prabakaran, F. Chen and Y. Q. Fu, Highly stable, love-mode surface acoustic wave biosensor using Au nanoparticle-MoS2-rGO nano-cluster doped polyimide nanocomposite for the selective detection of carcinoembryonic antigen, *Mater. Chem. Phys.*, 2020, **246**(1), 122800.
130 C. Li, J. Zhang, H. Xie, J. Luo, C. Fu, R. Tao, H. Li and Y. Fu, Highly Sensitive Love Mode Acoustic Wave Platform with SiO_2 Wave-Guiding Layer and Gold Nanoparticles for Detection of Carcinoembryonic Antigens, *Biosensors*, 2022, **12**(7), 536.

131 G. Moreau, N. N. Fourati, C. Zerrouki, H. Mouhsine, M. Montes, M. Port, M. S.-I. Veitía, J. F. Zagury and N. Yaakoubi, Surface Acoustic Wave Biosensors for the Quantification of TNF-α/SPD-304 Interaction, *Procedia Eng.*, 2016, **168**, 432–435.

132 P. Tang, Y. Wang, J. Huo and X. Lin, Love Wave Sensor for Prostate-Specific Membrane Antigen Detection Based on Hydrophilic Molecularly-Imprinted Polymer, *Polymer*, 2018, **10**(5), 563.

133 J. Lee, Y.-S. Choi, Y. Lee, H. J. Lee, J. N. Lee, S. K. Kim, K. Y. Han, E. C. Cho, J. C. Park and S. S. Lee, Sensitive and Simultaneous Detection of Cardiac Markers in Human Serum Using Surface Acoustic Wave Immunosensor, *Anal. Chem.*, 2011, **83**, 8629–8635.

134 K. Mitsakakis and E. Gizeli, Detection of multiple cardiac markers with an integrated acoustic platform for cardiovascular risk assessment, *Anal. Chim. Acta*, 2011, **699**, 1–5.

135 J. Luo, P. Luo, M. Xie, K. Du, B. Zhao, F. Pan, P. Fan, F. Zeng, D. Zhang, Z. Zheng and G. Liang, A new type of glucose biosensor based on surface acoustic wave resonator using Mn-doped ZnO multilayer structure, *Biosens. Bioelectron.*, 2013, **49**, 512–518.

136 V. Heitmann, B. Reiß and J. Wegener, in *Piezoelectric Sensors*, 2007, ch. 31, pp. 303–338, DOI: **10.1007/5346_031**.

137 S. Y. C. Tong, J. S. Davis, E. Eichenberger, T. L. Holland and V. G. Fowler, Staphylococcus aureus Infections: Epidemiology, Pathophysiology, Clinical Manifestations, and Management, *Clin. Microbiol. Rev.*, 2015, **28**, 603–661.

138 K. Tsougeni, G. Kaprou, C. M. Loukas, G. Papadakis, A. Hamiot, M. Eck, D. Rabus, G. Kokkoris, S. Chatzandroulis, V. Papadopoulos, B. Dupuy, G. Jobst, E. Gizeli, A. Tserepi and E. Gogolides, Lab-on-Chip platform and protocol for rapid foodborne pathogen detection comprising on-chip cell capture, lysis, DNA amplification and surface-acoustic-wave detection, *Sens. Actuators, B*, 2020, **320**(1), 128345.

139 Y. Q. Fu, J. K. Luo, N. T. Nguyen, A. J. Walton, A. J. Flewitt, X. T. Zu, Y. Li, G. McHale, A. Matthews, E. Iborra, H. Du and W. I. Milne, Advances in piezoelectric thin films for acoustic biosensors, acoustofluidics and lab-on-chip applications, *Prog. Mater. Sci.*, 2017, **89**, 31–91.

140 R. Tao, J. Reboud, H. Torun, G. McHale, L. E. Dodd, Q. Wu, K. Tao, X. Yang, J. T. Luo, S. Todryk and Y. Fu, Integrating microfluidics and biosensing on a single flexible acoustic device using hybrid modes, *Lab Chip*, 2020, **20**, 1002–1011.

141 H. Jin, J. Zhou, X. He, W. Wang, H. Guo, S. Dong, D. Wang, Y. Xu, J. Geng, J. K. Luo and W. I. Milne, Flexible surface acoustic wave resonators built on disposable plastic film for electronics and lab-on-a-chip applications, *Sci. Rep.*, 2013, **3**, 2140.

142 J. K. Luo, X. L. He, J. Zhou, W. B. Wang, W. P. Xuan, J. K. Chen, H. Jin, Y. Xu and S. R. Dong, Flexible and transparent surface acoustic wave microsensors and microfluidics, *Procedia Eng.*, 2015, **120**, 717–720.

143 T. Peng, L. Li, M. Zhou and F. Jiang, Concentration of Microparticles Using Flexural Acoustic Wave in Sessile Droplets, *Sensors*, 2022, **22**(3), 1269.

144 Y. Wang, Q. Zhang, R. Tao, J. Xie, P. Canyelles-Pericas, H. Torun, J. Reboud, G. McHale, L. E. Dodd, X. Yang, J. Luo, Q. Wu and Y. Fu, Flexible/Bendable Acoustofluidics Based on Thin-Film Surface Acoustic Waves on Thin Aluminum Sheets, *ACS Appl. Mater. Interfaces*, 2021, **13**, 16978–16986.

145 X. Chen, C. Zhang, B. Liu, Y. Chang, W. Pang and X. Duan, A self-contained acoustofluidic platform for biomarker detection, *Lab Chip*, 2022, **22**, 3817–3826.

146 J. C. Pyun, H. Beutel, J. U. Meyer and H. H. Ruf, Development of a biosensor for E. coli based on a flexural plate wave (FPW) transducer, *Biosens. Bioelectron.*, 1998, **13**, 839–845.

147 I. Y. Huang and M. C. Lee, Development of a FPW allergy biosensor for human IgE detection by MEMS and cystamine-based SAM technologies, *Sens. Actuators, B*, 2008, **132**, 340–348.

148 L. Lamanna, F. Rizzi, V. R. Bhethanabotla and M. De Vittorio, Conformable surface acoustic wave biosensor for E-coli fabricated on PEN plastic film, *Biosens. Bioelectron.*, 2020, **163**, 112164.

149 D. Chen, W. Ren, S. Song, J. Wang, W. Liu and P. Wang, The High Q Factor Lateral Field–Excited Thickness Shear Mode Film Bulk Acoustic Resonator Working in Liquid, *Micromachines*, 2016, **7**(12), 231.